

Article

What is the nature of interactions of BF_4^- , NO_3^- and ClO_4^- to Cu(II) complexes with Girard's T hydrazine? When can binuclear complexes be formed?

Tanja Keški#, Božidar #obelji#, Maja Gruden, Katarina An#elkovi#,
Andrej Pevec, Iztok Turel, Dušanka Radanovi#, and Matija Zlatar

Cryst. Growth Des., **Just Accepted Manuscript** • DOI: 10.1021/acs.cgd.9b00760 • Publication Date (Web): 15 Jul 2019

Downloaded from pubs.acs.org on July 15, 2019

Just Accepted

"Just Accepted" manuscripts have been peer-reviewed and accepted for publication. They are posted online prior to technical editing, formatting for publication and author proofing. The American Chemical Society provides "Just Accepted" as a service to the research community to expedite the dissemination of scientific material as soon as possible after acceptance. "Just Accepted" manuscripts appear in full in PDF format accompanied by an HTML abstract. "Just Accepted" manuscripts have been fully peer reviewed, but should not be considered the official version of record. They are citable by the Digital Object Identifier (DOI®). "Just Accepted" is an optional service offered to authors. Therefore, the "Just Accepted" Web site may not include all articles that will be published in the journal. After a manuscript is technically edited and formatted, it will be removed from the "Just Accepted" Web site and published as an ASAP article. Note that technical editing may introduce minor changes to the manuscript text and/or graphics which could affect content, and all legal disclaimers and ethical guidelines that apply to the journal pertain. ACS cannot be held responsible for errors or consequences arising from the use of information contained in these "Just Accepted" manuscripts.

1
2
3
4
5
6
7
8
9
10
11
12
13
14
15
16
17
18
19
20
21
22
23
24
25
26
27
28
29
30
31
32
33
34
35
36
37
38
39
40
41
42
43
44
45
46
47
48
49
50
51
52
53
54
55
56
57
58
59
60

What is the nature of interactions of BF_4^- , NO_3^- and ClO_4^- to Cu(II) complexes with Girard's T hydrazine? When can binuclear complexes be formed?

Tanja Keškić,[†] Božidar Čobeljić,[†] Maja Gruden,[†] Katarina Anđelković,[†] Andrej Pevec,[‡] Iztok Turel,[‡] Dušanka Radanović^{§} and Matija Zlatar^{*§}*

[†]Faculty of Chemistry, University of Belgrade, Studentski trg 12-16, 11000 Belgrade, Serbia.

[‡]Faculty of Chemistry and Chemical Technology, University of Ljubljana, Večna pot 113, 1000 Ljubljana, Slovenia.

[§]Department of Chemistry, Institute of Chemistry, Technology and Metallurgy, National Institute, University of Belgrade, Njegoševa 12, 11000 Belgrade, Serbia.

ABSTRACT: In the solid-state coordination chemistry, the coordination number of a metal center is not always unambiguously determined, as sometimes from the geometrical parameters it is not clear if ligands are directly bound to the central metal ion or they belong to the outer sphere of a complex. Nature of bonding between Cu(II) and weakly coordinated anions BF_4^- , NO_3^- and ClO_4^- are investigated by the combined crystallographic and computational study. It is shown that the synergy between the crystal structure determination and computational chemistry allows identification of all interactions present in crystals. Three new complexes, $[\text{CuLCl}]\text{BF}_4$ (**1**), $[\text{CuLCl}]\text{NO}_3$ (**2**) and $[\text{Cu}_2\text{L}_2\text{Cl}_2](\text{BF}_4)_2$ (**3**) with the same $[\text{CuLCl}]^+$ moiety ($\text{L}=(E)\text{-}N,N,N\text{-}$ trimethyl-2-oxo-2-(2-(1-(pyridin-2-yl)ethylidene) hydrazinyl)ethan-1-amin), were synthesized and characterized by single crystal X-ray diffraction methods and compared to the previously reported $[\text{CuLCl}]\text{ClO}_4$ (**4**). Energy decomposition analysis, non-covalent interaction index analysis, independent gradient model and the quantum theory of atoms in molecules are performed on the X-ray structures of these four complexes. The results revealed that in **1**, **2** and **4** BF_4^- , NO_3^- and ClO_4^- are weakly, but directly coordinated to the Cu(II) with bonds having high electrostatic character. In **3**, BF_4^- is the counter-anion, electrostatically bonded to the **L**. Furthermore, the present analysis rationalized the fact that only complex **3** is binuclear with bridging Cl^- ions.

1. INTRODUCTION

Design of molecular crystals requires an explicit understanding of different, intra- and inter-molecular interactions. Combination of the crystal structure determination and computational chemistry emerges as a powerful strategy for advancement in crystal engineering. Notably, the

1
2
3 application of computational chemistry tools allows precise determination of various interactions
4 present in crystals, that surpasses simple geometrical criteria that are frequently used. In solid-
5 state coordination chemistry, the coordination number of a metal center is typically specified
6 based only on the distance of surrounding ligands to the metal cation. Often this assumption is
7 appropriate. However, in the case of weakly coordinated anions, like tetrafluoroborate (BF_4^-),
8 nitrate (NO_3^-), or perchlorate (ClO_4^-) there is uncertainty whether in crystals they are directly
9 bound to the central metal ion or they belong to the outer sphere of a complex.^{1,2} If the central
10 metal ion is Cu(II), description of coordination geometries is particularly challenging.
11 Complexes of Cu(II) are typically subject to the Jahn-Teller types of distortions resulting in long
12 axial or apical metal-ligand contacts.^{3,4} Considering tetragonal Cu(II) complexes, with one or
13 two axial ligands with F, O or N donor atoms, it is assumed that ligand is bonded to Cu(II) if
14 Cu(II)-ligand distance is less than 2.4 Å.³ If the Cu(II)-ligand distance is larger than 2.8 Å, it is
15 assumed that Cu(II)-ligand interaction is of the van der Waals type.³ In the range 2.4-2.8 Å
16 ligand should be bonded electrostatically.³ In the case of chloride ligand, Cl^- is considered
17 bonded if Cu(II)-Cl distance is less than 2.8 Å and electrostatically bonded if the distance is
18 between 2.8 and 3.2 Å.³ The three types of Cu(II)-ligand interactions are referred by Halcrow as
19 genuine, secondary and van der Waals contacts.³ This division of Cu(II)-ligand interactions is
20 based solely on the sum of corresponding radii.
21
22
23
24
25
26
27
28
29
30
31
32
33
34
35
36
37
38
39
40
41
42
43

44 In this article, we address vagueness of the coordination of BF_4^- , NO_3^- and ClO_4^- to Cu(II) by
45 the combined crystallographic and computational study. For this study, three new complexes,
46 $[\text{CuLCl}]\text{BF}_4$ (**1**), $[\text{CuLCl}]\text{NO}_3$ (**2**) and $[\text{Cu}_2\text{L}_2\text{Cl}_2](\text{BF}_4)_2$ (**3**) with the same $[\text{CuLCl}]^+$ fragment
47 ($\text{L}=(E)\text{-}N,N,N\text{-trimethyl-2-oxo-2-(2-(1-(pyridin-2-yl)ethylidene)hydrazinyl)ethan-1-amin}$) were
48 synthesized and characterized by single crystal X-ray diffraction methods and compared to the
49
50
51
52
53
54
55
56
57
58
59
60

1
2
3 previously reported [CuLCl]ClO₄ (**4**).⁵ Structures of newly synthesized complexes **1-3**, as well
4
5 as, structure of **4**,⁵ are perfect examples of intricate bonding present in crystals of Cu(II)
6
7 complexes. Density functional theory (DFT) based analysis on the X-ray structures of these four
8
9 complexes containing the same inner-sphere cation and different anions are performed to
10
11 understand the nature of bonding between Cu(II) and weakly coordinated anions. Namely,
12
13 energy decomposition analysis,⁶⁻⁸ non-covalent interaction (NCI) index analysis,⁹ independent
14
15 gradient model (IGM)^{10,11} and the quantum theory of atoms in molecules (QTAIM)¹² are used to
16
17 identify all interactions present in the crystals of these complexes. This analysis helps in
18
19 understanding the coordination geometry around Cu(II) ion in crystals. Also, this study discerns
20
21 whether the self-assemblies of the complexes, as found in the crystals, are de facto polynuclear
22
23 complexes.
24
25
26
27
28
29

30 31 **2 EXPERIMENTAL**

32 33 **2.1 Materials and methods**

34
35 2-Acetylpyridine ($\geq 99\%$) and Girard's T reagent (99%) were obtained from Aldrich. IR
36
37 spectra were recorded on a Nicolet 6700 FT-IR spectrometer using the ATR technique in the
38
39 region 4000–400 cm⁻¹ (s-strong, m-medium, w-weak). Elemental analyses (C, H, and N) were
40
41 performed by standard micro-methods using the ELEMENTARVario ELIII C.H.N.S.O analyzer.
42
43

44 45 **2.2 Synthesis**

46
47 **2.2.1 Synthesis of ligand HLCl (*E*)-*N,N,N*-trimethyl-2-oxo-2-(2-(1-(pyridin-2-
48
49 yl)ethylidene)hydrazinyl)ethan-1-aminium-chloride.** The ligand HLCl was synthesized by the
50
51 reaction of Girard's T reagent (1.676 g, 1.00 mmol) and 2-acetylpyridine (1.120 mL, 1.00 mmol)
52
53 in methanol (50 mL). The reaction mixture was acidified with 3–4 drops of 2M HCl and was
54
55
56
57
58
59
60

1
2
3 refluxed for 2h at 85 °C. IR (cm⁻¹): 3387 (w), 3127 (m), 3090 (m), 3049 (m), 3016 (m), 2950 (s),
4
5 1700 (vs), 1612 (w), 1549 (s), 1485 (m), 1400 (m), 1300 (w), 1253 (w), 1200 (s), 1153 (w), 1135
6
7 (m), 1095 (w), 1073 (m), 975 (w), 944 (w), 914 (m), 748 (w), 683 (w). Elemental analysis calcd
8
9 for C₁₂H₁₉ClN₄O: C 53.23 %, H 7.07 %, N 20.69 %, found: C 53.42 %, H 7.12 %, N 20.77 %.

10
11
12 **2.2.2 Synthesis of [CuLCl]BF₄ (1) and [Cu₂L₂Cl₂](BF₄)₂ (3).** The mononuclear (1) and
13
14 binuclear (3) Cu(II) complexes were synthesized by the reaction of Cu(BF₄)₂·6H₂O (0.115 g,
15
16 0.30 mmol) and ligand HLCl (0.081 g, 0.30 mmol) in methanol (20 mL). The solution was
17
18 refluxed for 4h. After slow evaporation of the solvent in the refrigerator (~ 7°C) for ten days, two
19
20 kinds of green crystals suitable for X-ray analysis were formed. The main fraction corresponds to
21
22 compound 1, while complex 3 was obtained only in traces.

23
24
25
26 **2.2.3 Synthesis of [CuLCl]NO₃ (2).** Into a methanol solution (10 mL) of ligand HLCl (0.054
27
28 g, 0.20 mmol), Cu(NO₃)₂·3H₂O (0.050 g, 0.20 mmol) dissolved in 5 mL of methanol, was added.
29
30 The reaction mixture was refluxed for 4h. After refrigeration of the reaction solution at -8 °C for
31
32 a one week, green crystals suitable for X-ray analysis were formed. Yield: 72 mg (91 %). IR
33
34 (cm⁻¹): 3373 (vs), 3326 (m), 3271 (vs), 3106 (m), 3061 (m), 3031 (m), 1596 (vs), 1561 (m),
35
36 1529 (w), 1482 (s), 1443 (s), 1365 (m), 1307 (m), 1265 (w), 1196 (w), 1167 (m), 1118 (w), 1075
37
38 (w), 1048 (w), 1021 (w), 981 (w), 909 (w), 784 (s), 675 (w), 648 (w), 575 (w). Elemental
39
40 analysis calcd for C₁₂H₁₈ClCuN₅O₄: C 36.46 %, H 4.59 %, N 17.72 %, found: C 36.57 %, H 4.64
41
42 %, N 17.48 %.

43 44 45 46 **2.3 X-ray crystallography**

47
48
49 The molecular structures of complexes 1, 2, and 3 were determined by single-crystal X-ray
50
51 diffraction methods. Crystallographic data and refinement details are given in Supporting
52
53 Information (SI). Diffraction data for 1–3 were collected at 150 K for 1 and 3 and 293 K for 2
54
55
56
57
58
59
60

1
2
3 with Agilent SuperNova dual source diffractometer using an Atlas detector and equipped with
4 mirror-monochromated MoK α radiation ($\lambda = 0.71073 \text{ \AA}$). The data were processed by using
5 CrysAlis PRO.¹³ All the structures were solved using SIR-92¹⁴ (1 and 3) or SHELXS-97¹⁵ (2)
6 and refined against F^2 on all data by full-matrix least-squares with SHELXL-2016.¹⁶ All non-
7 hydrogen atoms were refined anisotropically. All other hydrogen atoms were included in the
8 model at geometrically calculated positions and refined using a riding model. The *ORTEP-3*¹⁷ for
9 Windows and *MERCURY*¹⁸ programs were used for graphical presentations. CCDC 1917721 (for
10 **1**), 1917722 (for **2**) and 1917723 (for **3**) contain the supplementary crystallographic data for this
11 paper. These data can be obtained free of charge from The Cambridge Crystallographic Data
12 Centre via www.ccdc.cam.ac.uk/data_request/cif.
13
14
15
16
17
18
19
20
21
22
23
24
25

26 **2.4 Computational details**

27
28 All calculations were performed using DFT formalism on the model systems constructed from
29 the corresponding crystal structures (structures **1-4**). For mononuclear complexes, the interaction
30 between [CuLCl]⁺ and the nearest counter-anions in the X-ray determined geometries of **1**, **2**, **3**
31 and **4** structures were studied. To understand the formation of binuclear complexes, the
32 interaction between two monomer units from the X-ray structures were investigated. In the X-ray
33 structures of **1** and **4**, BF₄⁻ and ClO₄⁻, respectively, are disordered. To see how the geometries of
34 anions influence the analysis, constrained geometry optimization of F atoms in the dimeric
35 structure of **1**, and O(perchlorate) atoms in the dimeric structure of **4** have been performed with
36 ORCA 4.1.1 program,^{19,20} using revPBE²¹ exchange-correlation functional with Grimme's third
37 generation dispersion energy correction²² and Becke-Johnson damping,²³ *i.e.* revPBE-D3
38 functional. Relativistic effects were accounted for by Zeroth-Order Regular Approximation
39 (ZORA) in the scalar-relativistic formulation.²⁴⁻²⁶ ZORA-def2-TZVP basis set for all atoms
40
41
42
43
44
45
46
47
48
49
50
51
52
53
54
55
56
57
58
59
60

1
2
3 and the resolution-of-the-identity approximation in the Split-RI-J variant and the scalar
4 relativistically recontracted SARC/J Coulomb fitting sets have been used.^{27–29}
5
6

7
8 The nature of the interaction between chosen fragments was analyzed with the aid of the
9 extended transition state energy decomposition scheme (EDA)^{6–8} as implemented in ADF
10 program package.^{30–32} The interaction energy between fragments is decomposed into four
11 chemically meaningful components: $E_{\text{int}}=E_{\text{elst}}+E_{\text{Pauli}}+E_{\text{orb}}+E_{\text{disp}}$. The term E_{elst} is the quasi-
12 classical electrostatic interaction between the fragments; E_{Pauli} is the repulsive Pauli interaction
13 between occupied orbitals on the two fragments and is accounting for a steric interaction; E_{orb} is
14 a stabilizing contribution due to the charge transfer and polarization; E_{disp} is the dispersion
15 energy correction. Additionally, natural orbitals for chemical valence (NOCV)^{33,34}
16 decomposition of the electron density deformation was performed to elucidate different density
17 transfer channels and to quantify their importance as an energy contribution to the E_{orb} . Charge
18 flow between the fragments was quantified with Hirshfeld charge analysis.³⁵ For energies, the
19 general gradient approximated (GGA) in the form of BP86,^{36–38} PBE³⁹ and revPBE²¹ were used,
20 with Grimme's third generation dispersion energy correction²² and Becke–Johnson damping,²³
21 *i.e.* BP86-D3, PBE-D3, and revPBE-D3 functionals. Furthermore, dispersion corrected meta-
22 GGA, M06L^{40,41} functional with zero damping (parameters: $s_6=1.0$, $s_{r,6}=1.325$, $s_8=0.0$) was used.
23 ZORA in the scalar-relativistic formulation^{24,25} has been used. An all-electron triple- ζ Slater-type
24 orbitals plus one polarization function (TZP) basis set was employed for all atoms.
25
26
27
28
29
30
31
32
33
34
35
36
37
38
39
40
41
42
43
44
45

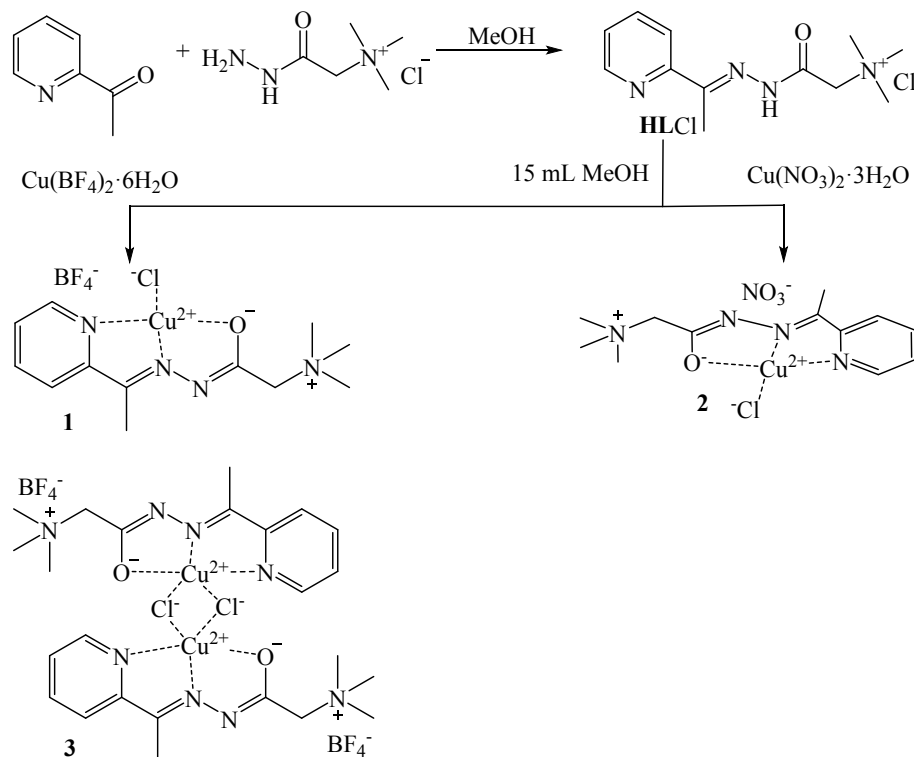
46
47 Non-covalent interactions between fragments had been identified with the aid of the Non-
48 Covalent Interactions Index (NCI)⁹ and Independent Gradient Model (IGM)^{10,11} methods.
49 Interactions between fragments were also analyzed within the framework of Bader's Quantum
50 Theory of Atoms in Molecules (QTAIM).¹² NCI, IGM and QTAIM analyses were performed by
51
52
53
54
55
56
57
58
59
60

1
2
3 Multiwfn software 3.6⁴² on the wave functions generated at the self-consistent (SC) revPBE-
4 NL/ZORA-def2-TZVP level of theory. revPBE-NL⁴³ is the non-local (NL) density-dependent
5 dispersion functional.⁴⁴ DFT-NL calculations were carried out with ORCA 4.1.1 program^{19,20}
6
7 with the resolution-of-the-identity approximation in the Split-RI-J variant and the scalar
8 relativistically recontracted SARC/J Coulomb fitting sets.²⁷⁻²⁹ NCI model is based on the
9
10 visualization of the isosurfaces of the reduced density gradient(s) colored by the product of the
11 sign of the second eigenvalue of the electron density Hessian and electron density ($\text{sign}(\lambda_2)*\rho$).
12
13 Isosurfaces are colored with “Blue-Green-Red” color scheme, so that the strong attractive
14 interactions (negative $\text{sign}(\lambda_2)*\rho$) are blue, weak attractive interactions and van der Waals
15 interactions are green ($\text{sign}(\lambda_2)*\rho$ close to zero), and steric repulsion is red (positive $\text{sign}(\lambda_2)*\rho$).
16
17 Localized interactions are disk-shaped, while delocalized interactions are depicted as diffused
18 surfaces. Thus, the shape and color of the isosurfaces are informative of the type and spatial
19
20 localization of noncovalent interactions. IGM model is based on calculating $\delta g = g^{\text{IGM}} - g$, where
21
22 g^{IGM} is the density gradient calculated as the sum of the absolute value of the density gradient of
23 each atom in their free-states and g is the true density gradient. In the IGM model, δg can be
24
25 defined only in the inter-fragment region, and isosurfaces of δg^{inter} colored by the $\text{sign}(\lambda_2)*\rho$ are
26
27 used to identify various inter-fragment interactions analogously to the NCI method. IGM
28
29 isosurfaces are more rounded shaped compared to the NCI isosurfaces. QTAIM is based on the
30
31 topological analysis of the electron density. The electron density, its Laplacian, total energy
32
33 density, the potential energy density, and the kinetic energy density at inter-fragment bond
34
35 critical points were used for additional study of chemical bonding between fragments.
36
37
38
39
40
41
42
43
44
45
46
47
48
49
50
51
52
53
54
55
56
57
58
59
60

3. RESULTS AND DISCUSSION

3.1. General

The ligand, (*E*)-*N,N,N*-trimethyl-2-oxo-2-(2-(1-(pyridin-2-yl)ethylidene)hydrazinyl)ethan-1-aminium-chloride (**HLCl**), was obtained from the condensation reaction of 2-acetylpyridine and Girard's T reagent in methanol (Scheme 1). In the reaction of ligand **HLCl** with $\text{Cu}(\text{BF}_4)_2 \cdot 6\text{H}_2\text{O}$ in a 1:1 molar ratio in methanol, mixture of mononuclear (**1**) and binuclear (**3**) Cu(II) complexes, was obtained (Scheme 1). Changing polarity of solution using different solvent or mixture of solvents, as well as, changing the molar ratio of reactants, did not affect obtained results (additional Experimental details are in SI). The reaction of **HLCl** with $\text{Cu}(\text{NO}_3)_2 \cdot 3\text{H}_2\text{O}$ in a 1:1 molar ratio, in methanol, gives mononuclear Cu(II) complex **2**, with composition $[\text{CuLCl}]\text{NO}_3$ (Scheme 1).



Scheme 1 Schematic presentation of the synthesis of ligand (**HLCl**) and complexes **1**, **2** and **3**

1
2
3
4
5 The ligand **HLCl** has recently been used for the preparation of mononuclear $[\text{CuLCl}]\text{ClO}_4$ (**4**)
6 and binuclear $[\text{Cu}_2\text{L}_2(\mu_{-1,1}\text{-N}_3)_2](\text{ClO}_4)_2$ complexes.⁵ Both complexes were found to be good
7 catalysts in the synthesis of *N*-arylatedimidazoles and benzimidazoles.⁵ The **HLCl** ligand
8 possesses positively charged quaternary ammonium fragment and can exist either in protonated
9 monocationic form or as a deprotonated zwitterionic ligand. In mononuclear complex **4** and
10 binuclear $[\text{Cu}_2\text{L}_2(\mu_{-1,1}\text{-N}_3)_2](\text{ClO}_4)_2$ complex hydrazone based ligand is zwitterionic and the
11 distorted square-planar and square-pyramidal geometries of Cu(II) ions, respectively, have been
12 established by X-ray crystallography. However, if long Cu...O(perchlorate) contacts are
13 considered as weak coordinative bonds Cu(II) in **4** is the distorted square-pyramid, while in
14 $[\text{Cu}_2\text{L}_2(\mu_{-1,1}\text{-N}_3)_2](\text{ClO}_4)_2$ is of pseudo-octahedral geometry. Furthermore, in the crystals of
15 mononuclear complex **4**, complex cations $[\text{CuLCl}]^+$ of square-planar geometry are linked
16 through in-plane coordinated chloride anions so to mimic a dimeric structure $[\text{Cu}_2\text{L}_2\text{Cl}_2](\text{ClO}_4)_2$
17 with the distance of approximately 3.6 Å between the Cu(II) centres.⁵ Considering the crystal
18 structures of related mononuclear Cu(II) complexes, we have found relatively short
19 Cu(II)...Cu(II) separations, nearly 4.0 Å, in two structures $[\text{Cu}(\text{HL}^2)\text{Cl}_2\text{CuHL}^2\text{Cl}(\text{H}_2\text{O})]\text{Cl}$
20 ($\text{HL}^2 = 2\text{-formylpyridine semicarbazone}$)⁴⁵ and $[\text{CuHL}^4\text{Cl}_2]$ ($\text{HL}^4 = 2\text{-pyridine-carboxaldehyde 4-}$
21 $\text{dimethyl-aminobenzoylhydrazone}$).⁴⁶ However, in the other mononuclear Cu(II) considered, the
22 distance between the closest metal centers exceeds 6.4 Å (*vide infra*).⁴⁷⁻⁴⁹ Cu(II) ions in herein
23 reported structures **1** and **2** are either in a distorted square-planar or in a distorted square-
24 pyramidal environment. The coordination geometry of **1** and **2** depends whether BF_4^- and NO_3^-
25 are considered as counter-anions, or they are coordinated to the Cu(II). Both **1** and **2**, similarly
26 as **4**, can be considered as dimeric structures linked through in-plane coordinated chloride anions
27
28
29
30
31
32
33
34
35
36
37
38
39
40
41
42
43
44
45
46
47
48
49
50
51
52
53
54
55
56
57
58
59
60

with the distance between the closest Cu(II) centers of approximately 3.6 and 3.8 Å, respectively. In binuclear complex **3**, BF_4^- is not bonded to Cu(II) but is linked via hydrogen bonds to the **L** (*vide infra*). In the binuclear complexes $[\text{Cu}_2\text{L}_2(\mu_{-1,1}\text{-N}_3)_2](\text{ClO}_4)_2$ and **3** the distance between the closest Cu(II) centers is approximately 3.4 Å.

3.2 The crystal structures of $[\text{CuLCl}]\text{BF}_4$ (**1**), $[\text{CuLCl}]\text{NO}_3$ (**2**) and $[\text{Cu}_2\text{L}_2\text{Cl}_2](\text{BF}_4)_2$ (**3**) complexes

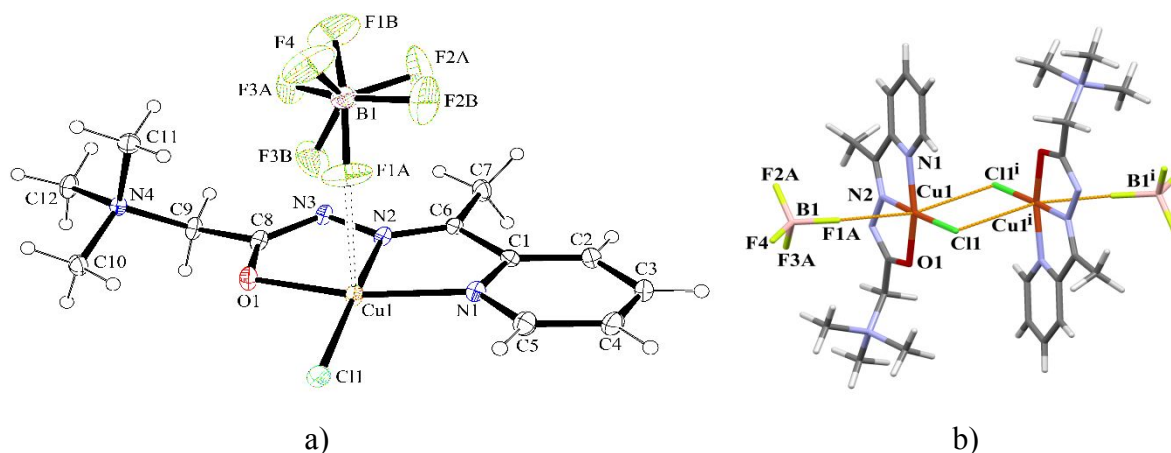


Figure 1. a) ORTEP presentation of the $[\text{CuLCl}]\text{BF}_4$ (**1**). Thermal ellipsoids are drawn at the 30% probability level. Long contact $\text{Cu}\cdots\text{F}$ is represented as a dashed line. b) View of the dimeric unit of **1** of pseudo-octahedral geometry. Long contacts $\text{Cu}\cdots\text{F}$ and $\text{Cu}\cdots\text{Cl}$ are represented as orange lines. BF_4^- anions suffer from positional disorder. Symmetry code *i* stands for $2-x, -y, 2-z$.

The molecular structures of $[\text{CuLCl}]\text{BF}_4$ (**1**), $[\text{CuLCl}]\text{NO}_3$ (**2**) and $[\text{Cu}_2\text{L}_2\text{Cl}_2](\text{BF}_4)_2$ (**3**) with atom numbering schemes are presented in Figures 1a, 2 and 3, respectively. The selected bond lengths and bond angles for **1**, **2** and **3** are given in SI (Table S2). The structural parameters

1
2
3 correlating the geometry of related mononuclear^{5,45-49} (**1**, **2** and **4-10**) and binuclear⁵⁰⁻⁵² (**3**, **11-**
4
5 **14**) Cu(II) complexes with hydrazone-based NNO-donor ligands are listed in Table 1.

6
7
8 Complex **1** crystallizes in the monoclinic centrosymmetric space group $P2_1/c$, with the
9
10 asymmetric unit comprising one complex cation $[\text{CuLCl}]^+$ and statistically disordered BF_4^-
11
12 anion. The complexes **1**, **2** and **4**⁵ are isostructural. The complex cation features a four-
13
14 coordinate Cu(II) center with the NNO donor set of tridentate zwitterionic ligand **L** and the Cl^-
15
16 ion supplementing the fourth coordination site (Figure 1a). The coordination geometry around
17
18 Cu(II) may be described as a distorted square planar with τ_4 parameter⁵³ of 0.17 for **1** ($\tau_4 =$
19
20 $360^\circ - (\alpha + \beta) / 141^\circ$, where α and β are the two largest angles around the central atom). The
21
22 values of τ_4 can range from 1.00 for a perfect tetrahedral geometry to zero for a perfect square
23
24 planar. Intermediate structures, including trigonal pyramidal and seesaw, fall within the range of
25
26 0 to 1.00. The tridentate NNO coordination of **L** to Cu(II) ion generates two five-membered
27
28 chelate rings (Cu-N-C-C-N and Cu-N-N-C-O) fused along the Cu1-N2 bond. The chelate rings
29
30 are non-coplanar, as indicated by the dihedral angle of 3.5° . Similarly, as in the case of **4**, the
31
32 complex units of **1** are organized into $[\text{Cu}_2\text{L}_2\text{Cl}_2](\text{BF}_4)_2$ dimers (Figure 1b) in which the
33
34 symmetry related Cu(II) ions of tetragonally elongated octahedral geometry are separated by
35
36 $3.5990(4)$ Å. In the crystals of **1**, the complex molecules are arranged in layers parallel with the
37
38 $(0\ 0\ 1)$ lattice plain by means of intermolecular C-H...F and C-H...Cl hydrogen bonds (*cf.* SI).
39
40 The adjacent layers are packed via C7-H7A...F2A and C12-H12C...F3A hydrogen bonds into the
41
42 three-dimensional supramolecular structure. The Cu-N_{py} ($2.0023(19)$ Å), Cu-N_{imine} ($1.9308(18)$
43
44 Å), Cu-O ($1.9806(15)$ Å) and Cu-Cl ($2.2141(6)$ Å) distances are similar to those for copper(II)
45
46 complexes where the metal ions are coordinated to the same type of atoms (Table 1). As
47
48 expected, the complexes **6-10** show slightly longer Cu-O_{am} ($2.035(2)$ - $2.137(2)$ Å) distances
49
50
51
52
53
54
55
56
57
58
59
60

compared to the distances (1.953(3)-1.990(3)Å) observed in complexes **1-5** and **11-14** having deprotonated amide-O bound copper(II).

Table 1 Structural parameters correlating the geometry of related mono- and binuclear Cu(II) complexes with hydrazone-based NNO-donor ligands

Complexes	CN ^a	Cu---Cu (Å)	Bond lengths (Å)		τ_4/τ_5 _b	ρ^c (Å)	Cu-Cl-Cu (°)	Ref.
			In-plane	Axial				
Mononuclear								
[CuLCl]BF ₄ (1)	4	3.5990(4)	Cu1-N1 2.0023(19) Cu1-N2 1.9308(18) Cu1-O1 1.9806(15) Cu1-Cl1 2.2141(6)		0.17			This work
[CuLCl]NO ₃ (2)	4	3.7973(5)	Cu1-N1 2.0031(18) Cu1-N2 1.9239(18) Cu1-O1 1.9777(15) Cu1-Cl1 2.2056(6)		0.19			This work
[CuLCl]ClO ₄ (4)	4	3.5793(8)	Cu1-N1 2.005(4) Cu1-N2 1.931(4) Cu1-O1 1.990(3) Cu1-Cl1 2.2175(14)		0.15			5
[CuL ¹ Cl(DMSO)] ^d (5)	5	6.5328(5)	Cu-N1 2.043(2) Cu-N2 1.942(2) Cu-O1 1.988(2) Cu-Cl 2.2354(7)	Cu-O2 2.242(2)	0.08	0.2205(3)		47
[Cu(HL ²)Cl ₂ CuHL ² Cl(H ₂ O)]Cl ^{e, f} (6)	5	3.902(1)	Cu1B-N2B 2.022(2) Cu1B-N1B 1.956(2) Cu1B-O1B 2.035(2) Cu1B-Cl2B 2.2186(12) Cu1A-N2A 2.037(2) Cu1A-N1A 1.948(2) Cu1A-O1A 2.039(2) Cu1A-Cl1A 2.1983(10)	Cu1B-Cl1B 2.5737(9) Cu1A-O2A 2.397(2)	0.04	0.2329(4)		45
[CuHL ³ Cl ₂] ^{e, g} (7)	5	7.0803(5)	Cu-N1 2.044(2) Cu-N2 1.971(2) Cu-O1 2.137(2) Cu-Cl2 2.2212(8)	Cu-Cl1 2.4344(8)	0.22	0.3292(3)		47
[CuHL ⁴ Cl ₂] ^{e, h} (8)	5	4.023(1)	Cu1-N1 2.044(2) Cu1-N2 1.961(2) Cu1-O1 2.063(2) Cu1-Cl1 2.2053(9)	Cu1-Cl2 2.5128(10)	0.16	0.2753(4)		46
[CuHL ⁵ Cl ₂] ^{e, i} (9)	5	6.650(2)	Cu1-N3 2.031(2) Cu1-N2 1.965 (2) Cu1-O1 2.059 (2) Cu1-Cl1 2.2110 (7)	Cu1-Cl2 2.4892 (9)	0.06	0.3553(3)		48
[CuHL ⁶ Cl ₂] ^{e, j} (10)	5	6.447(1)	Cu1-N1 2.0390 (16) Cu1-N2 1.9638 (15) Cu1-O1 2.0872 (14) Cu1-Cl2 2.2116 (6)	Cu1-Cl3 2.4655 (7)	0.22	0.3018(2)		49

Binuclear

[Cu ₂ L ₂ Cl ₂](BF ₄) ₂ (3)	5	3.3644(6)	Cu1-N1 2.023(3)		0.17	0.1820(4)	85.78(3)	This work
			Cu1-N2 1.931(3)	Cu1-Cl1 ⁱⁱ 2.6800(9)				
			Cu1-O1 1.977(2)					
			Cu1-Cl1 2.2408(8)					
[Cu ₂ (L ⁷) ₂ (Cl) ₂] ^k (11)	5	3.4000(3)	Cu1-N1 2.0008(14)		0.17	0.1034(2)	83.94(2)	⁵⁰
			Cu1-N2 1.9347(14)	Cu1-Cl1 ⁱⁱⁱ 2.8033(5)				
			Cu1-O1 1.9623(12)					
			Cu1-Cl1 2.2425(4)					
[Cu ₂ (L ⁸) ₂ (Cl) ₂] ^l (12)	5	3.3691(4)	Cu1-N1 2.0084(18)		0.08	0.1611(3)	85.03(2)	⁵¹
			Cu1-N2 1.9374(16)	Cu1-Cl1 ⁱⁱ 2.7158(6)				
			Cu1-O1 1.9636(14)					
			Cu1-Cl1 2.2430(6)					
[Cu ₂ (L ⁹) ₂ (Cl) ₂] ^m (13)	5	3.4085(8)	Cu1-N1 2.017(3)		0.02	0.2468(4)	88.33(3)	⁵²
			Cu1-N2 1.932(3)	Cu1-Cl1 ^{iv} 2.6206(10)				
			Cu1-O1 1.953(3)					
			Cu1-Cl1 2.2572(9)					
[Cu ₂ (L ¹⁰) ₂ (Cl) ₂] ⁿ (14)	5	3.2926(5)	Cu1-N1 2.0003(17)		0.11	0.1878(3)	84.56(2)	⁵²
			Cu1-N2 1.9431(18)	Cu1-Cl1 ^{iv} 2.6248(6)				
			Cu1-O1 1.9569(15)					
			Cu1-Cl1 2.2523(6)					

Symmetry codes: ii= $-x, -y, -z+1$; iii = $-x+1, -y+2, -z+1$; iv = $-x+1, -y+1, -z$.

^aCN= Coordination number. ^bFor Cu(II) complexes of CN = 4 the τ parameter has been calculated using the equation $\tau_4 = 360^\circ - (\alpha + \beta) / 141^\circ$, where α and β are the two largest angles around the central atom. For Cu(II) complexes of CN = 5 the τ parameter has been calculated using the equation $\tau_5 = (\beta - \alpha) / 60$, where β and α are the two largest angles around the central atom. ^c ρ (Å) is the distance of metal ion from the mean basal plane of square pyramid toward the apical ligand. ^dL¹= 2-formylpyridine-*para*-nitro-phenyl hydrazone. ^eComplexes having keto-O bound copper(II). ^fHL²= 2-formylpyridine semicarbazone. ^gHL³= 2-formylpyridine-*para*-chloro-phenyl hydrazone. ^hHL⁴= 2-pyridine-carboxaldehyde 4-dimethyl-aminobenzoylhydrazone. ⁱHL⁵ = condensation product of 2-acetylpyridine and acetyl hydrazide. ^jHL⁶ = condensation product of 2-formylpyridine and acetyl hydrazide. ^kL⁷ = methyl 2-pyridyl ketone semicarbazone. ^lL⁸ = 2-benzoylpyridine-3-methoxybenzhydrazone. ^mL⁹ = condensation product of adamantane-1-carbohydrazide and 2-acetylpyridine. ⁿL¹⁰ = condensation product of adamantane-1-carbohydrazide and di(2-pyridyl) ketone.

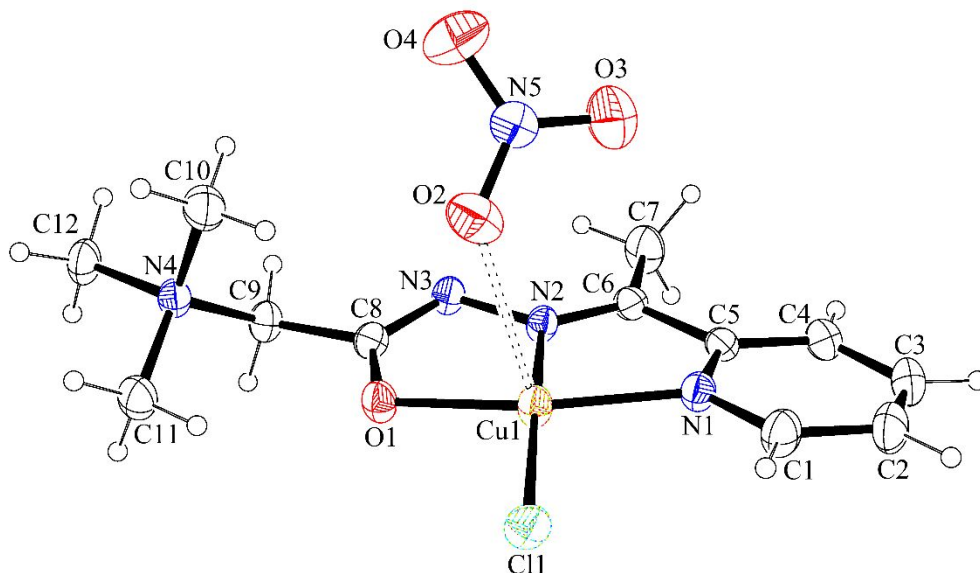


Figure 2. ORTEP presentation of the $[\text{CuLCl}]\text{NO}_3$ (**2**). Thermal ellipsoids are drawn at the 30% probability level. Long contact $\text{Cu}\cdots\text{O}$ is represented as a dashed line.

Complex **2** also crystallizes in the monoclinic space group $P2_1/c$. The asymmetric unit of **2** comprises the complex cation $[\text{CuLCl}]^+$ and NO_3^- anion (Figure 2). Complexes **1** and **2** show greater distortion from perfect square planar configuration than complex **4**, as indicated by the calculated τ_4 parameters of 0.17 and 0.19 vs 0.15 (Table 1). Crystal packing of **2** is similar to that of **1** and **4**. In the crystals of **2** the complex molecules are connected by means of intermolecular $\text{C-H}\cdots\text{O}$ and $\text{C-H}\cdots\text{Cl}$ hydrogen bonds into the layer parallel with the (0 0 1) lattice plain (*cf.* SI). The adjacent layers are packed via $\text{C12-H12A}\cdots\text{O4}$ hydrogen bond to form a three-dimensional supramolecular structure. In complexes **1**, **2**, **4**⁵ and **6**⁴⁵ the formation of dimeric units $[\text{Cu}_2\text{L}_2\text{Cl}_2](\text{BF}_4)_2$, $[\text{Cu}_2\text{L}_2\text{Cl}_2](\text{NO}_3)_2$, $[\text{Cu}_2\text{L}_2\text{Cl}_2](\text{ClO}_4)_2$, and $[\text{Cu}(\text{HL}^2)\text{Cl}_2\text{CuHL}^2\text{Cl}(\text{H}_2\text{O})]^+$, respectively, is accomplished by linking the metal centers through in-plane coordinated chloride anions which leads to short separations between the closest Cu atoms ($\text{Cu}\cdots\text{Cu}$ is in the range 3.5793(8)-3.902(1)Å) in comparison to those observed for **5**, **7**, **9** and **10**. In complex **8** relatively short $\text{Cu}\cdots\text{Cu}$ distance of 4.023(1) Å is achieved by π -stacking

of the neighboring hydrogen bonded dimers. The other mononuclear Cu(II) complexes (**5**, **7**, **9** and **10**) listed in Table 1, show significantly longer Cu...Cu separations.

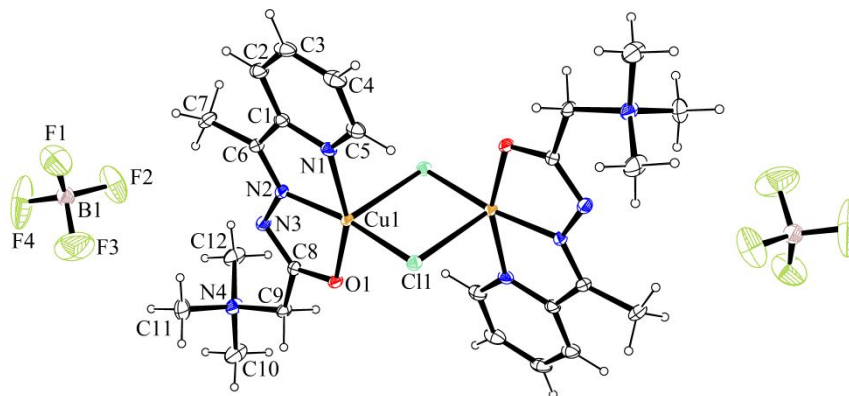


Figure 3. ORTEP presentation of the $[\text{Cu}_2\text{L}_2\text{Cl}_2](\text{BF}_4)_2$ (**3**). Thermal ellipsoids are drawn at the 30% probability level. Unlabeled part of the dimeric molecule and one BF_4^- counter anion are generated by symmetry operation $-x, -y, 1-z$.

Complex **3** crystallizes in the monoclinic space group $P2_1/n$, with the asymmetric unit comprising one Cu(II) center, zwitterionic ligand **L**, one Cl^- ion and BF_4^- counter anion. The crystal structure displays a centrosymmetric binuclear complex with the crystallographically independent Cu1 center being coordinated to three donor atoms (N1, N2 and O1) of **L** and two bridging chlorine atoms (Cl1 and Cl1 at $-x, -y, -z+1$) (Figure 3). The Cu(II) ion in **3** adopts a distorted square pyramidal geometry with an index of trigonality (τ_5)⁵⁴ of 0.17 ($\tau_5 = (\beta - \alpha)/60$, where β and α are the two largest angles around the central atom; τ_5 is 0 for regular square based pyramidal geometry and 1.00 for regular trigonal bipyramidal geometry). The square base of the Cu(II) center is formed by pyridyl (N1) and imine (N2) nitrogen atoms and enolate oxygen (O1) of **L** and one chloride ion (Cl1), while the apical position is occupied by the

1
2
3 symmetry related chloride ion at $-x, -y, -z+1$. The chloride ion bridges in an asymmetric (basal–
4 apical) fashion so that the in-plane and axial Cu–Cl bond lengths are significantly different,
5
6 $\text{Cu1–Cl1} = 2.2408(8) \text{ \AA}$ and $\text{Cu1–Cl1}^{\text{ii}} = 2.6800(9) \text{ \AA}$ (where ii stands for $-x, -y, -z+1$). The
7
8 asymmetric bridging mode of chlorido ligands has also been established in complexes **11-14**
9
10 (Table 1). In **3** and **11-14**, the four-membered Cu_2Cl_2 bridging units are constrained to be planar
11
12 by the presence of the symmetry element with the Cu...Cu separations ranging from 3.2926(5) to
13
14 3.4085(8) \AA and Cu–Cl–Cu angles from 83.94(2) to 88.33(3) $^\circ$. The complexes **3** and **11** show the
15
16 same degree of trigonal distortion of regular square pyramidal geometry. For the other binuclear
17
18 complexes listed in Table 1, τ_5 value varies from 0.02 to 0.11, indicating that these structures are
19
20 closer to the ideal square pyramidal configuration. The Cu(II) ions in **3** and **11-14** are displaced
21
22 by distance ρ of 0.1034(2)-0.2468(4) \AA from the basal N, N, O, Cl plane towards the apical
23
24 chlorine atom. In the crystal structure of complex **3** the dimeric molecules self-assemble within
25
26 the layer parallel with the (0 1 0) lattice plane by means of $\pi \cdots \pi$ stacking interactions between
27
28 the adjacent aromatic rings of L and C–H...Cl hydrogen bonds. The BF_4^- anions, placed in
29
30 between the adjacent layers are involved in the intermolecular C–H...F hydrogen bonds and serve
31
32 to connect the neighboring layers, as well as, to support stacking of the aromatic rings along the
33
34 [100] (*cf.* SI).

3.3 DFT calculations on monomer units

35
36
37 To investigate the nature of bonding of counter-anions in the structures of the complexes **1-4**,
38
39 energy decomposition analysis has been performed, and the results are summarized in Table 2.
40
41 Note that the inner sphere is taken from corresponding X-ray structures (**1-4**), and in this section,
42
43 interaction with counter-anions is emphasized. In the case of **1**, the geometry of BF_4^- does not
44
45
46
47
48
49
50
51
52
53
54
55
56
57
58
59
60

1
2
3 influence the analysis (Table S7 in SI summarizes the analysis on the structure with optimized F
4 atoms). In the X-ray structure of **4**, the geometry of ClO_4^- deviates markedly from the expected
5 tetrahedral shape. Optimization of O atoms recovers tetrahedral geometry of ClO_4^- .
6
7
8 Consequently, there are some differences in energy components between the two considered
9 structures, but general trends in the interactions in **4**-- ClO_4^- are the same. In the following
10 discussion results of the **4**-- ClO_4^- with optimized O(perchlorate) will be given, while the results
11 on the structures where all atoms are extracted from the crystal structure of **4** are reported in SI.
12
13
14
15
16
17
18
19 (Table S8, Figure S5 in SI)
20

21 In all the structures, the most dominant stabilizing term is electrostatic interaction between the
22 fragments. It accounts for approximately 75-85% of the stabilization. Pauli repulsion is small,
23 because of the large separation between the fragments. Dispersion correction is non-negligible
24 (approximately 4-7% of the stabilization). The choice of density functional approximation is not
25 affecting the results, with only small numerical differences. The only differences are present in
26 the case of M06L-D3 because M06L in its parameterization already encompasses dispersion.
27
28
29 Therefore, in this case, dispersion corrections are negligible. Consequently, Pauli repulsion in
30
31
32
33
34
35
36
37
38
39
40
41
42
43
44
45
46
47
48
49
50
51
52
53
54
55
56
57
58
59
60

Table 2. Energy decomposition analysis of $[\text{CuLCl}]^+ \text{X}^-$ in monomer structures **1**, **2**, **3** and **4** at different levels of theory; energy components are given in kcal/mol; Δq is Hirshfeld charge, transferred between fragments; coordinates of all atoms are extracted from corresponding X-ray structures except in the case of **4** where O(perchlorate) atoms are optimized at revPBE/def2-TZVP level of theory because of disorder in the X-ray structure.

$[\text{CuLCl}]^+ \text{X}^-$	Energy Component	BP86-D3	PBE-D3	revPBE-D3	M06L-D3
1 -- BF_4^-	E_{elst}	-64.15	-64.57	-64.78	-63.72
	E_{Pauli}	13.00	10.86	14.16	5.34
	E_{orb}	-13.43	-13.43	-13.47	-14.74
	E_{disp}	-5.46	-3.22	-5.81	-0.79
	E_{int}	-70.04	-70.35	-69.91	-73.91
	Δq	0.08	0.07	0.07	0.07
2 -- NO_3^-	E_{elst}	-71.39	-71.73	-71.91	-71.15
	E_{Pauli}	16.34	14.23	17.89	7.44
	E_{orb}	-18.77	-18.98	-18.73	-18.39
	E_{disp}	-6.45	-3.84	-7.15	-0.77
	E_{int}	-80.27	-80.32	-79.89	-82.88
	Δq	0.25	0.21	0.20	0.14
3 -- BF_4^-	E_{elst}	-66.52	-66.59	-66.61	-66.25
	E_{Pauli}	4.47	2.52	4.38	0.42
	E_{orb}	-8.02	-8.14	-8.22	-8.47
	E_{disp}	-2.96	-1.9	-3.33	-0.66
	E_{int}	-73.7	-74.11	-73.77	-74.96
	Δq	0.03	0.03	0.03	0.02
4 -- ClO_4^-	E_{elst}	-62.16	-62.40	-62.56	-62.02
	E_{Pauli}	11.72	9.28	12.71	3.68
	E_{orb}	-12.78	-12.91	-12.81	-13.58
	E_{disp}	-7.89	-4.55	-8.20	-1.01
	E_{int}	-71.11	-70.58	-70.86	-72.93
	Δq	0.09	0.09	0.09	-0.08

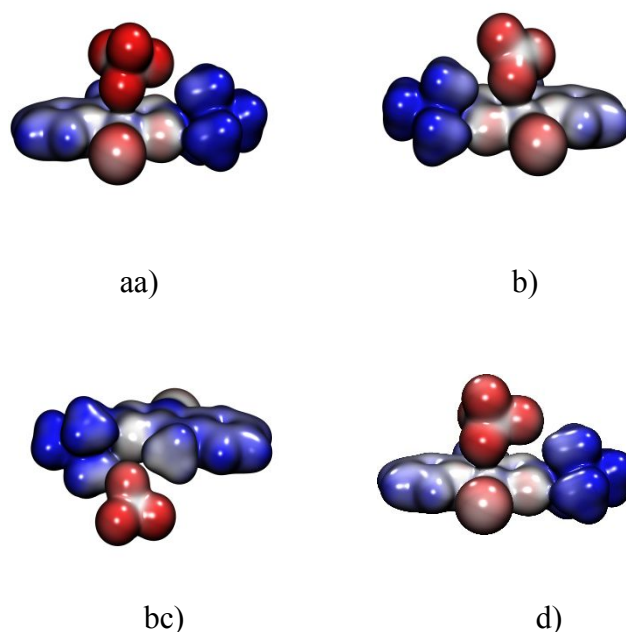


Figure 4. Electrostatic potential surfaces (at 0.01 au) from -0.13 (red) to $+0.13$ (blue) a.u. of monomeric units $[\text{CuLCl}]^+--\text{X}^-$ a) **1**-- BF_4^- b) **2**-- NO_3^- c) **3**-- BF_4^- d) **4**-- ClO_4^- .

The significance of the electrostatic stabilization is evident because of the charged fragments and is further illustrated in the electrostatic potential surfaces, Figure 4. The color code in Figure 4 is “Red-White-Blue”. It ranges from deep red, indicating negatively charged regions, to deep blue, positively charged regions. The counter-anions carry most of the negative charge. Positive charge is delocalized in $[\text{CuLCl}]^+$ moiety. The most positive region is $\text{N}(\text{CH}_3)_3$ group from the side chain of the **L**.

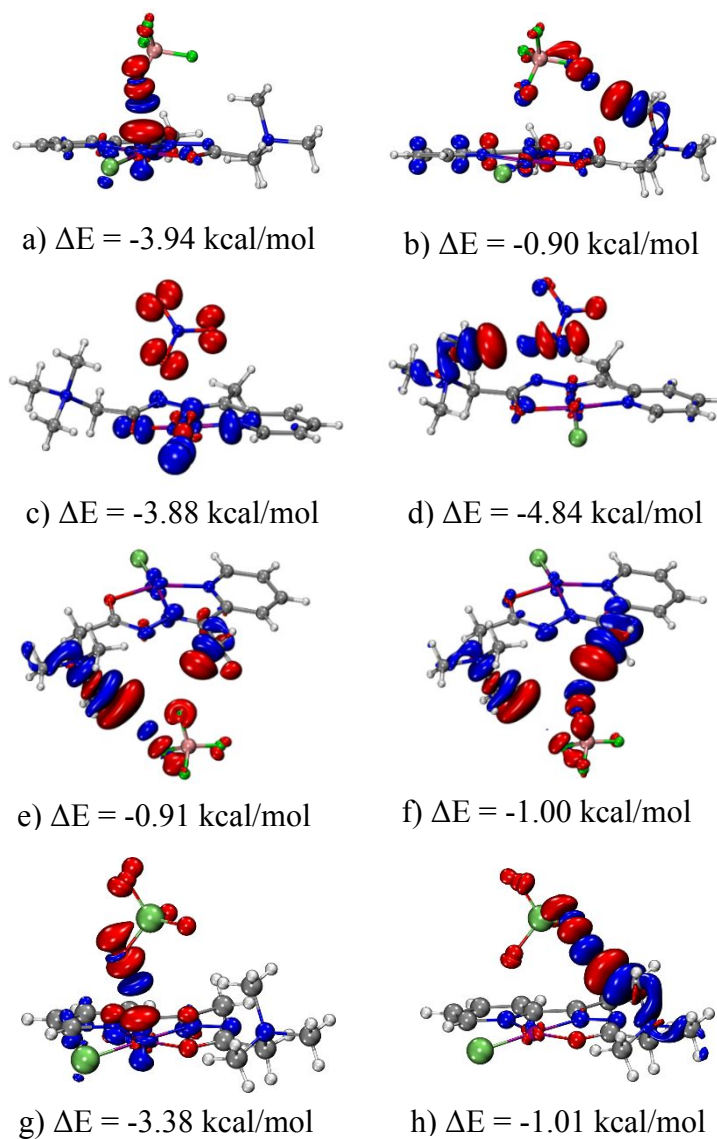
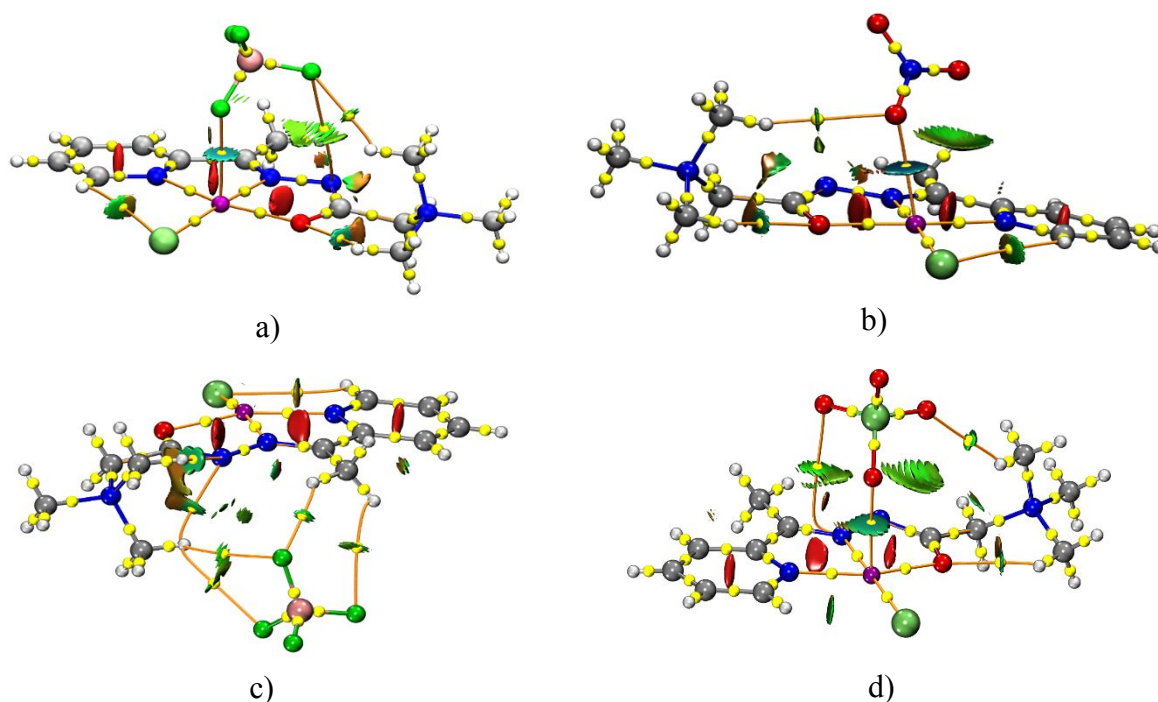


Figure 5. Most important covalent deformation density channels from NOCV analysis of $[\text{CuLCl}]^+ \cdots \text{X}^-$ interaction; a) **1** $\cdots \text{BF}_4^-$ metal-ligand (isovalue 0.001 a.u.) b) **1** $\cdots \text{BF}_4^-$ hydrogen bond (isovalue 0.0003 a.u.) c) **2** $\cdots \text{NO}_3^-$ metal-ligand (isovalue 0.001 a.u.) d) **2** $\cdots \text{NO}_3^-$ hydrogen bond (isovalue 0.0003 a.u.) e) and f) **3** $\cdots \text{BF}_4^-$ hydrogen bond (isovalue 0.0002 a.u.) g) **4** $\cdots \text{ClO}_4^-$ metal-ligand (isovalue 0.001 a.u.) h) **4** $\cdots \text{ClO}_4^-$ hydrogen bond (isovalue 0.0003 a.u.). Red/blue color represent electron outflow/inflow.

1
2
3 The preceding analysis shows clearly a prominent role of electrostatics in the interaction
4 between $[\text{CuLCl}]^+$ and counter-anions. In the case of **1**, **3**, and **4** this is additionally confirmed
5 with a small charge transfer, Δq in Table 2, between the fragments. However, in **2**, the charge
6 transfer is non-negligible, Table 2. Furthermore, E_{orb} , that often indicates covalency,⁵⁵ in all four
7 cases, contributes between 10-20% to the stabilization. Nevertheless, E_{orb} incorporates both the
8 effects of covalency (charge transfer between the fragments) and polarization. To clarify the
9 contribution of sole covalency, NOCV analysis has been performed. The most important density
10 deformation channels related to the covalency are depicted in Figure 5. Two types of covalent
11 interactions are found. The first one is metal-ligand covalency, *i.e.* ligand-to-metal charge
12 transfer present in **1**, **2** and **4**. The second type of covalent bonding is found in all structures and
13 is a covalent part of the hydrogen bonding between counter-anion and $\text{N}(\text{CH}_3)_3$ group. In all the
14 molecules, covalency is of minor importance, and polarization, *i.e.* electron density redistribution
15 on one fragment due to the presence of another one is dominating to the E_{orb} .
16
17
18
19
20
21
22
23
24
25
26
27
28
29
30
31
32

33 Detailed noncovalent interactions present in these systems are shown in Figure 6. NCI plots
34 show different interactions as distinctly colored and shaped regions. Strong attractive interactions
35 are blue, weak attractive interactions and van der Waals interactions are green, and steric
36 repulsion is red. Localized interactions are disk-shaped, while delocalized interactions are
37 depicted as diffused surfaces. In all four molecules, interactions in $[\text{CuLCl}]^+$ fragments are
38 identified: red disks in the middle of the two chelate rings, and the middle of the pyridine ring
39 indicate ring-strain; weak intramolecular hydrogen bonds between Cl^- and pyridine CH, and
40 between O1 and methyl group in $\text{N}(\text{CH}_3)_3$ group from the side chain of the L, are identified as
41 small green disks. Electrostatic interactions between counter-anions and Cu(II) in **1**, **2** and **4** are
42 shown as blue-green disks. In **3** BF_4^- and L are connected by hydrogen bonds (interactions
43
44
45
46
47
48
49
50
51
52
53
54
55
56
57
58
59
60

1
2
3 between BF_4^- and $\text{N}(\text{CH}_3)_3$ and between BF_4^- and C7H). Hydrogen bonding between counter-
4
5 anions and $\text{N}(\text{CH}_3)_3$ is present also in **1**, **2** and **4**. In these three molecules, there are also van der
6
7 Waals interactions between anions and chelate Cu-N-N-C-O rings.
8
9



38 **Figure 6.** Three dimensional NCI plots for a) **1**-- BF_4^- b) **2**-- NO_3^- c) **3**-- BF_4^- d) **4**-- ClO_4^- .
39
40 Isosurfaces (isovalue $s=0.4$) are colored in range $-0.03 < \text{sign}(\lambda_2) \cdot \rho < 0.02$ (“Blue-Green-Red”
41
42 color scheme). Bond paths, connecting bond critical points (yellow spheres) and nuclear critical
43
44 points (coinciding with atoms) are shown as orange lines.
45
46
47
48
49
50
51
52
53
54
55
56
57
58
59
60

Intermolecular interactions are also seen in IGM plots, Figure 7. In **1**, BF_4^- is bonded electrostatically with Cu(II), there is a hydrogen bonding between BF_4^- and $\text{N}(\text{CH}_3)_3$ and van der Waals interaction between BF_4^- and N3 of the Cu-N-N-C-O chelate ring. In **2** there are a strong electrostatic $\text{NO}_3^- \cdots \text{Cu}(\text{II})$ interaction, hydrogen bonding between NO_3^- and $\text{N}(\text{CH}_3)_3$ group, and evident anion- π van der Waals interactions between NO_3^- and Cu-N-N-C-O chelate ring. The situation in **4** is equivalent. In **3** there are two non-equivalent regions of hydrogen bonding between BF_4^- and $[\text{CuLCl}]^+$ fragment.

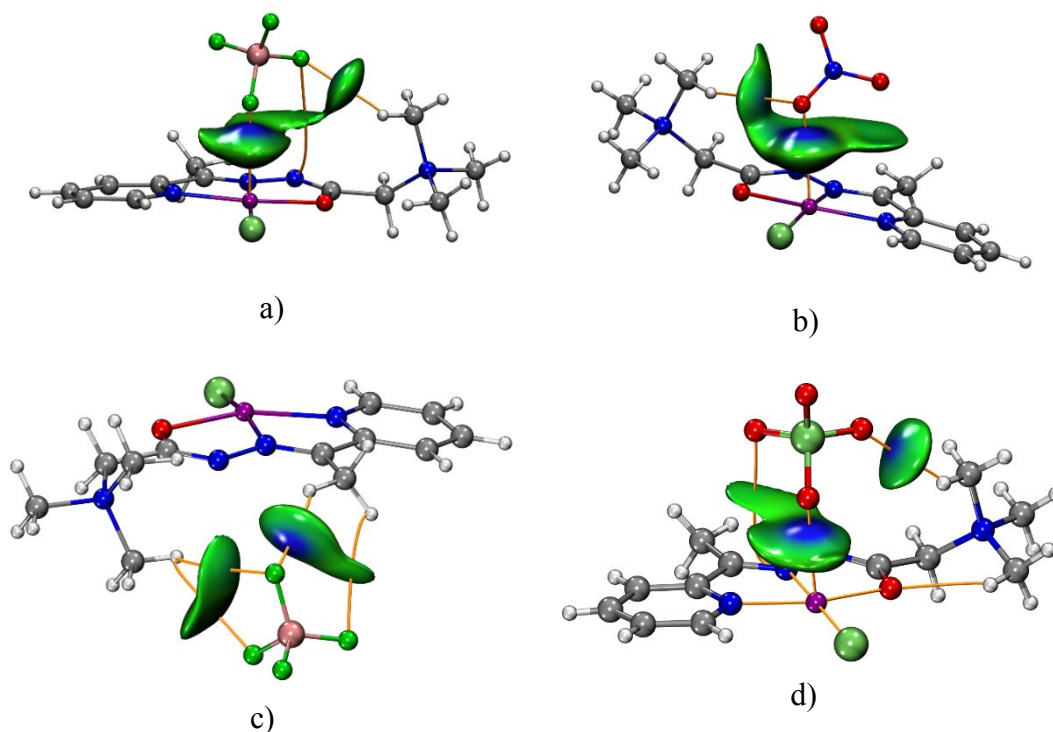


Figure 7. IGM plots for a) **1**-- BF_4^- b) **2**-- NO_3^- c) **3**-- BF_4^- d) **4**-- ClO_4^- ; isosurfaces of δg^{inter} (isovalue 0.004) colored by $\text{sign}(\lambda_2) \cdot \rho$ (range -0.05 to 0.05, “Blue-Green-Red” color scheme). Interfragment bond paths are shown as orange lines.

1
2
3 All the interactions are also identified in the framework of Bader's QTAIM method, with the
4 presence of corresponding critical points and bond paths (Figure 6 and 7 and Figure S7 in SI).
5
6 The topological properties of the electron density in bond critical points (Table S9 in SI)
7 confirms ionic nature of bonding between counter-anions and Cu(II), as well as, additional weak
8 hydrogen bonding between counter-anions and [CuLCl]⁺ fragment. IGM plots of δg^{inter} around
9 Cu(II) ion in **1**, **2** and **4** (Figure S6 in SI) show distinction between metal-ligand in-plane bonds
10 (Cu-N1, Cu-N2, Cu-O1 and Cu-Cl1) and Cu(II)-anion bonds. Metal-ligand in-plane bonds are
11 typical coordination bonds, while bonding with anions is obviously weaker but definitively
12 present.
13
14
15
16
17
18
19
20
21
22
23

24 All these results, taking into account both covalent and all noncovalent interactions, suggests
25 that in structures **1**, **2** and **4** anions are weakly coordinatively bound to Cu(II) with high ionic
26 character, while in **3** hydrogen bonding is responsible for the position of counter-anion.
27
28
29
30
31
32

33 **3.4 DFT study of binuclear complexes**

34
35 As indicated before, regardless of reaction conditions (additional Experimental details are in
36 SI), only complex **3** has been obtained as binuclear species. However, in **1**, **2** and **4** monomeric
37 units in the crystal are placed in a way that two Cu(II) ions are on somewhat shorter distance
38 than if the units are completely separated. Therefore, we performed DFT calculations to analyze
39 interactions between units in all four complexes.
40
41
42
43
44
45
46

47 Energy decomposition analysis of the formation of dimeric structures from monomer
48 complexes is given in Table 3. Geometries of BF_4^- and ClO_4^- does not influence the analysis
49 (Table S10 in SI summarizes the analysis on the structure **1--1** with optimized F atoms, and
50
51
52
53
54
55
56
57
58
59
60

Table S11 of the analysis of the structure **4** with all atoms taken from the X-ray structure of **4**).

Table 3. Energy decomposition analysis of [CuLCIX] $_2$ [CuLCIX] dimeric structures of **1**, **2**, **3** and **4** at different levels of theory; energy components are given in kcal/mol; Δq is Hirshfeld charge, transferred between fragments; coordinates of all atoms are extracted from corresponding X-ray structures except in the case of **4** where O(perchlorate) atoms are optimized at revPBE/def2-TZVP level of theory because of disorder in the X-ray structure.

[CuLCIX] $_2$ [CuLCIX]	Energy Component	BP86-D3	PBE-D3	revPBE-D3	M06L-D3
(BF $_4^-$) 1 -- 1 (BF $_4^-$)	E $_{elst}$	-20.03	-20.55	-20.46	-18.07
	E $_{Pauli}$	32.34	28.67	35.04	13.64
	E $_{orb}$	-15.49	-15.55	-15.21	-18.21
	E $_{disp}$	-21.5	-12.11	-21.66	-2.93
	E $_{int}$	-24.67	-19.54	-22.29	-25.57
	Δq	0.00	0.00	0.00	0.00
(NO $_3^-$) 2 -- 2 (NO $_3^-$)	E $_{elst}$	-9.34	-9.65	-9.69	-8.59
	E $_{Pauli}$	19.70	15.90	21.69	2.94
	E $_{orb}$	-11.24	-11.30	-11.12	-14.76
	E $_{disp}$	-20.77	-11.71	-20.63	-2.93
	E $_{int}$	-21.65	-16.76	-19.75	-23.34
	Δq	0.00	0.00	0.00	0.00
3	E $_{elst}$	-44.26	-44.43	-44.03	-42.02
	E $_{Pauli}$	56.91	54.49	59.91	41.63
	E $_{orb}$	-24.37	-24.36	-23.86	-26.71
	E $_{disp}$	-15.62	-8.53	-15.68	-1.88
	E $_{int}$	-27.34	-22.84	-23.66	-28.98
	Δq	0.00	0.00	0.00	0.00
(ClO $_4^-$) 4 -- 4 (ClO $_4^-$)	E $_{elst}$	-21.78	-22.21	-22.11	-20.04
	E $_{Pauli}$	33.23	29.73	35.67	15.74
	E $_{orb}$	-16.19	-16.25	-15.92	-18.93
	E $_{disp}$	-20.49	-11.55	-20.50	-2.93
	E $_{int}$	-25.22	-20.28	-22.85	-26.16
	Δq	0.00	0.00	0.00	0.00

From first sight, one can see a prominent role of the dispersion in interaction energies. As in the case of monomers, different density functional approximations give consistent results. The only exception is M06L-D3, where a dispersion, contained in the functional form, clearly lowers E $_{Pauli}$ while D3 part is only a further correction to the energy. Electrostatic attraction is bringing

two neutral monomers together in parallel displaced manner, (Figure S8 in SI). Covalency seems negligible in all four analyzed model binuclear structures, as the net charge transfer between two monomers, Δq , Table 3, is zero. NOCV analysis, Fig. 8, establishes that only in **3**, covalent σ bond between Cu-Clⁱⁱ brings considerable stabilization (it brings around 12% of the stabilization).

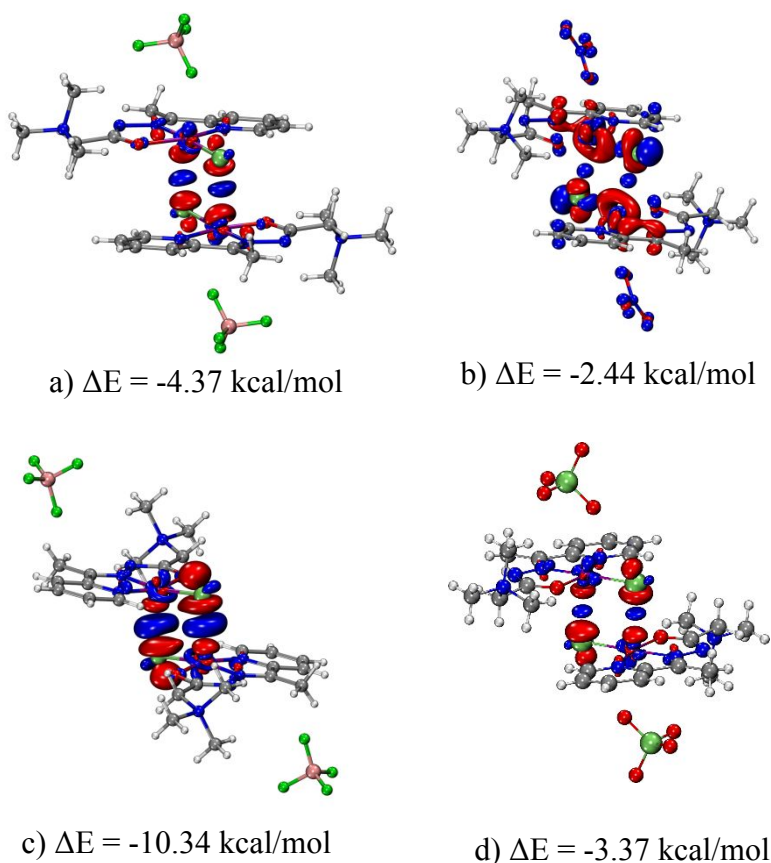


Figure 8. Most important covalent deformation density channels from NOCV analysis of [CuLCIX]--[CuLCIX] interactions; a) **1**--**1** (isovalue 0.001 a.u.) b) **2**--**2** (isovalue 0.0002 a.u.) c) **3** (isovalue 0.001 a.u.) d) **4**--**4** (isovalue 0.0008 a.u.). Red/blue color represent electron outflow/inflow.

Table 4 Influence of various dispersion corrections (Grimme's D3, Grimme's D4, non-local density dependent non-self-consistent (NL) and non-local density-dependent self-consistent (SCNL) functionals) to the revPBE/ZORA-def2-TZVP interaction energies of [CuLCIX]--[CuLCIX] in dimer structures of **1**, **2**, **3** and **4**. Comparison with results of revPBE-D3/TZP results is also given. All the energies are given in kcal/mol.

CuLCIX]--[CuLCIX]	Energy	revPBE ^a	revPBE-D3 ^a	revPBE-D4 ^a	revPBE-NL ^a	revPBE-SCNL ^a	revPBE ^{b,c}	revPBE-D3 ^{b,c}
1-1	E _{int}	0.28	-21.38	-21.13	-21.03	-21.50	-0.63 (0.74)	-22.29 (-20.92)
	E _{disp}	0.00	-21.66	-21.41	-21.32	-21.78	0.00	-21.66
1-1 (F-opt)^d	E _{int}	0.13	-21.53	-21.25	-21.19	-21.66	-0.75 (0.64)	-22.41 (-21.02)
	E _{disp}	0.00	-21.66	-21.38	-21.32	-21.79	0.00	-21.66
2-2	E _{int}	2.23	-18.40	-17.57	-17.42	-17.89	0.88 (2.99)	-19.75 (-17.64)
	E _{disp}	0.00	-20.63	-19.80	-19.65	-20.12	0.00	-20.63
3	E _{int}	-8.15	-23.84	-25.50	-25.29	-25.58	-7.98 (-6.64)	-23.66 (-22.33)
	E _{disp}	0.00	-15.68	-17.35	-17.14	-17.43	0.00	-15.68
4-4	E _{int}	1.50	-19.00	-18.98	-18.73	-19.18	1.04 (2.24)	-19.47 (-18.06)
	E _{disp}	0.00	-20.50	-20.48	-20.32	-20.68	0.00	-20.50
4-4 (O-opt)^e	E _{int}	-1.22	-21.72	-21.56	-21.32	-21.76	-2.35 (-0.67)	-22.85 (21.17)
	E _{disp}	0.00	-20.50	-20.34	-20.10	-20.34	0.00	-20.50

^aCalculations with ORCA program package. ^bCalculations with ADF program package. ^cResults in brackets are relative to unrestricted monomers. ^dF atoms of BF₄⁻ optimized. ^eO atoms of ClO₄⁻ optimized.

To further understand the importance of dispersion, the interaction energies were also calculated with ORCA program package using revPBE-D3/ZORA-def2-TZVP level of theory, as well as the Grimme's fourth generation dispersion energy correction (revPBE-D4⁵⁶) and the non-self-consistent and self-consistent non-local density-dependent dispersion functional (revPBE-NL and revPBE-SCNL,⁴³ respectively). In Table 4, the results at revPBE/TZP level of theory from Table 3 are also summarized, where the E_{int} is given both relative to the quasi-restricted

1
2
3 fragments (as done in the energy decomposition analysis, Table 3) and relative to the
4 electronically fully relaxed unrestricted monomers. The difference is around 1 kcal/mol. All the
5 results in Table 4 are consistent. revPBE results here are considered as “dispersion-free”.⁵⁷ We
6 see that without dispersion, the interaction energy of two monomer units in the dimer of **2** are
7 positive. In the case of dimers of **1** and **4**, interaction energies are close to zero or positive (in the
8 range approximately from -2 to +1 kcal/mol). Only in the case of **3**, interaction energy, even
9 without dispersion, is negative.

10
11
12 Interestingly, in all four systems, interaction energies between monomers are similar (from -17
13 kcal/mol to -25 kcal/mol). However, the nature of the interactions is different. Energy
14 decomposition analysis (Table 3), coupled with careful NOCV analysis (Figure 8) and
15 comparison of dispersion-corrected with “dispersion-free” results (Table 4), allow estimation of
16 various contributions to the interaction energies, namely contribution of electrostatics,
17 covalency, polarization and dispersion. In the case of **3**, most of the stabilization comes from the
18 electrostatics (53% of stabilization). Covalency brings around 12% of the stabilization,
19 polarization approximately 16% and dispersion around 18%. In the case of dimers of **1** and **4**
20 electrostatics and dispersion are of similar importance (both around 35% of the stabilization).
21 Polarization contributes around 20% to the stabilization and covalency is of minor importance
22 (around 5%). Dimer of **2** is mainly stabilized by dispersion interactions (50% of stabilization),
23 electrostatics and polarization provide both around 22% of stabilization, and covalency is of
24 minor importance (5% of stabilization).
25
26
27
28
29
30
31
32
33
34
35
36
37
38
39
40
41
42
43
44
45
46
47
48
49
50
51
52
53
54
55
56
57
58
59
60

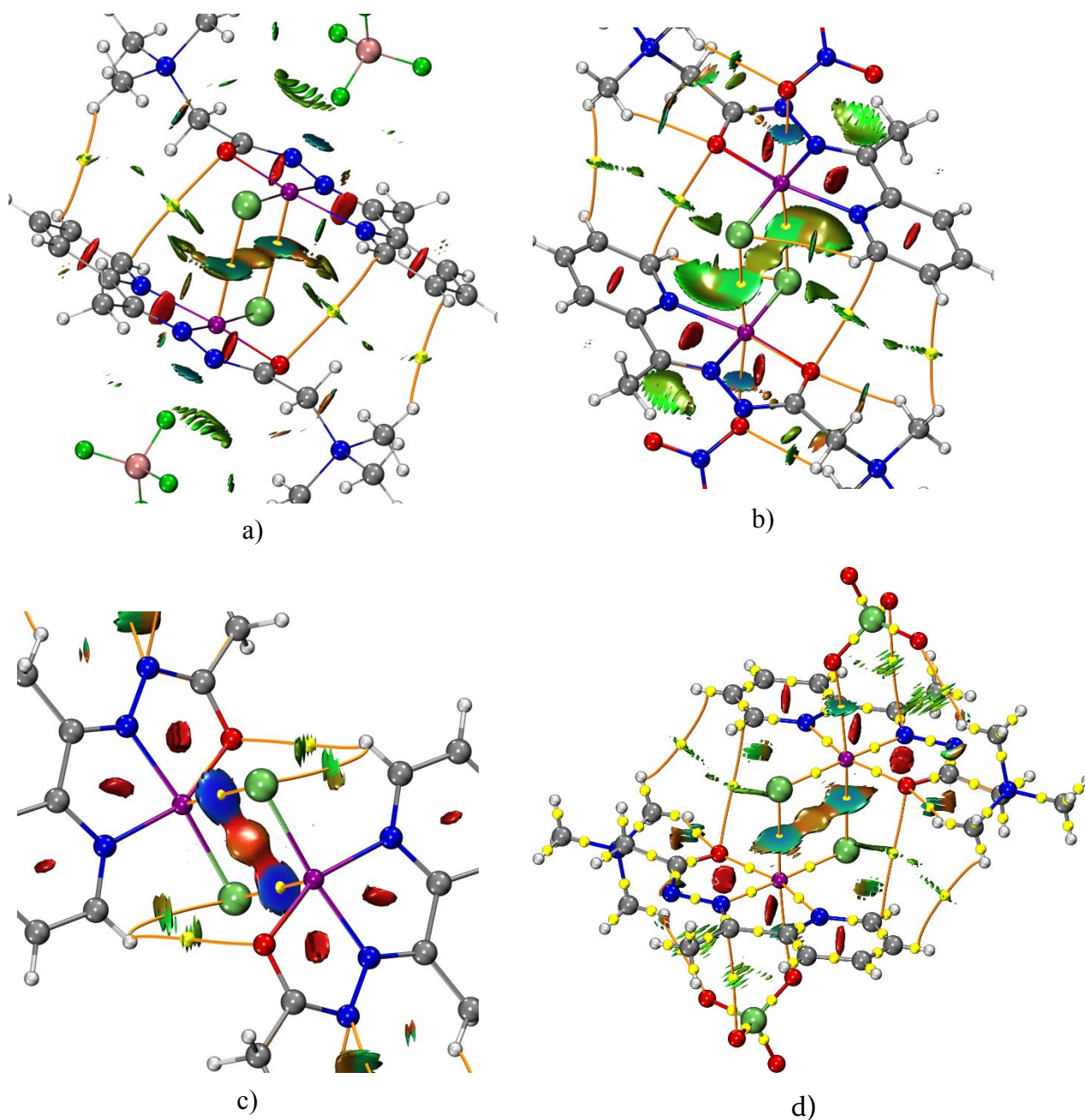


Figure 9. Three dimensional NCI plots for a) 1--1 b) 2--2 c) 3 d) 4--4. Isosurfaces (isovalue $s=0.4$) are colored in range $-0.03 < \text{sign}(\lambda_2) \rho < 0.02$ ("Blue-Green-Red" color scheme). Interfragment bond paths, connecting bond critical points (yellow spheres) and nuclear critical (coinciding with atoms) points are shown as orange lines.

1
2
3
4
5 Detailed noncovalent interactions between monomers are depicted in Figure 9 (NCI plots) and
6 Figure 10 (IGM plots). Strong Cu-Clⁱⁱ interactions are apparent in **3** - strong blue disks in NCI
7 plot and blue region in IGM plot, together with orange-red area in NCI plot, indicating strain in
8 formed Cu-Clⁱⁱ-Cuⁱⁱ-Cl ring. These Cu-Clⁱ interactions are weaker in **1** and **4**, revealed in NCI
9 and IGM plots by greener color. In **2** Cu-Clⁱ interactions are of the van der Waals type (diffuse
10 green surface). IGM plots showing only interactions around Cu(II) (Figure S9 in SI) reveal that
11 in **3** Cl⁻ acts as bridging ligand and confirms that in **2** Cu-Clⁱ interactions are of the van der
12 Waals type. Cu-Clⁱ interactions in **1** and **4** are in between these two. Additional attractive
13 interactions are found in all four dimers. Two types of van der Waals interactions are
14 encountered. The first one is between pyridine on one monomer and N(CH₃)₃ group of the other
15 monomer. The second is between pyridine and O1. Topological properties of the electron density
16 (Figure S10, Table S12 in SI) additionally confirm these types of interactions between monomer
17 units.
18
19
20
21
22
23
24
25
26
27
28
29
30
31
32
33
34

35 Results of the energy decomposition analysis and analysis of the non-covalent interactions
36 assert that only **3** has clear dimer structure, in accordance with experimental findings. In the
37 other three cases, two monomers mainly interact via van der Waals attractive forces, explaining
38 shortest Cu-Cu contact in **3**.
39
40
41
42
43
44
45
46
47
48
49
50
51
52
53
54
55
56
57
58
59
60

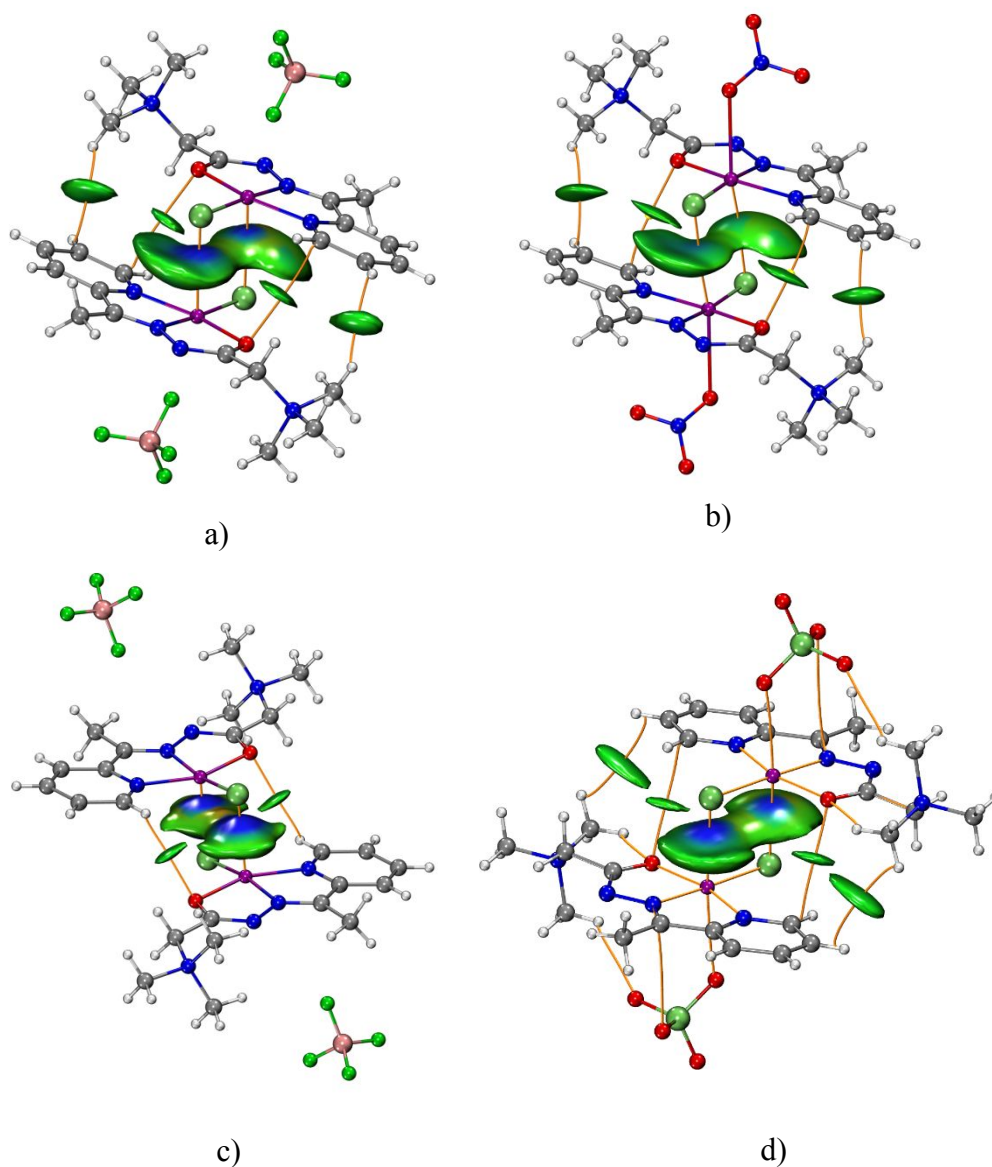


Figure 10. Isosurfaces of δg^{inter} (isovalue 0.004) coloured by $\text{sign}(\lambda^2)\rho$ (range -0.05 to 0.05, “Blue-Green-Red” color scheme) for a) 1--1 b) 2--2 c) 3 d) 4--4. Interfragment bond paths are shown as orange lines.

4. CONCLUSIONS

The complexes $[\text{CuLCI}]\text{BF}_4$, $[\text{CuLCI}]\text{NO}_3$ and $[\text{Cu}_2\text{L}_2\text{Cl}_2](\text{BF}_4)_2$ have been synthesized and characterized by X-ray crystallographic analysis. The structures of $[\text{CuLCI}]\text{BF}_4$ and $[\text{CuLCI}]\text{NO}_3$ are analogue to the previously reported $[\text{CuLCI}]\text{ClO}_4$. Geometries around Cu(II) ion in mononuclear complexes can be described either as distorted square planar or as distorted square pyramidal. Coordination around Cu(II) depends on the nature of bonding of BF_4^- , NO_3^- and ClO_4^- to the Cu(II) ion. In other words, coordination geometry will depend on whether the BF_4^- , NO_3^- and ClO_4^- are considered as counter-anions or ligands. DFT calculations revealed that in all three mononuclear complexes, they are weakly coordinatively bound to Cu(II), with high ionic character. Hence, their structural formulas could also be written as: $[\text{CuLCIBF}_4]$, $[\text{CuLCINO}_3]$ and $[\text{CuLCIClO}_4]$. It is noteworthy to mention that these ligands are weakly bonded, and in solution, they might dissociate, hence, *e.g.* conductivity measurements in solution will not give an accurate picture of what the structures would be in crystals. In binuclear $[\text{Cu}_2\text{L}_2\text{Cl}_2](\text{BF}_4)_2$, BF_4^- is clearly a counter-anion, and its position is a consequence of hydrogen bonding with **L**. In accordance with the experimental findings, DFT calculations establish that only complex **3** exist as binuclear species, where two Cu(II) ions are connected via bridging Cl^- ions. Complexes **1**, **2** and **4** form structures where units are held together via attractive van der Waals forces.

The present study shows that ambiguity about actual coordination number in the real crystal structures of coordination compounds can be overcome with the aid of DFT based calculations, like analysis of interaction energy components, NCI and IGM plots, and QTAIM analysis.

1
2
3
4
5 ASSOCIATED CONTENT
6
7

8 **Supporting Information.** Supporting information for X-ray crystallography; Additional
9 experimental details for the synthesis of **1** and **3**; Additional computational results for
10 mononuclear structures; Additional computational results for dimer structures.
11
12
13
14
15
16
17
18

19
20 AUTHOR INFORMATION
21

22 **Corresponding Authors**
23

24
25 *radanovic@chem.bg.ac.rs
26

27
28 *matijaz@chem.bg.ac.rs
29
30

31 **Author Contributions**
32

33
34 The manuscript was written through the contributions of all authors. All authors have given
35 approval to the final version of the manuscript.
36
37
38

39
40 ACKNOWLEDGMENT
41

42 This work was supported by the Ministry of Education, Science and Technological
43 Development of the Republic of Serbia (Grants OI 172035 and OI 172055) and the Slovenian
44 Research Agency (P-0175).
45
46
47
48
49
50
51
52
53
54
55
56
57
58
59
60

REFERENCES

- (1) Díaz-Torres, R.; Alvarez, S. Coordinating ability of anions and solvents towards transition metals and lanthanides. *Dalt. Trans.* **2011**, *40* (40), 10742 DOI: 10.1039/c1dt11000d.
- (2) Rosenthal, M. R. The myth of the non-coordinating anion. *J. Chem. Educ.* **1973**, *50* (5), 331 DOI: 10.1021/ed050p331.
- (3) Halcrow, M. A. Jahn–Teller distortions in transition metal compounds, and their importance in functional molecular and inorganic materials. *Chem. Soc. Rev.* **2013**, *42* (4), 1784–1795 DOI: 10.1039/C2CS35253B.
- (4) Gruden-Pavlović, M.; Zlatar, M.; Schläpfer, C.-W.; Daul, C. DFT study of the Jahn–Teller effect in Cu(II) chelate complexes. *J. Mol. Struct. THEOCHEM* **2010**, *954* (1–3), 80–85 DOI: 10.1016/j.theochem.2010.03.031.
- (5) Milenković, M. R.; Papastavrou, A. T.; Radanović, D.; Pevec, A.; Jagličić, Z.; Zlatar, M.; Gruden, M.; Vougioukalakis, G. C.; Turel, I.; Anđelković, K.; et al. Highly-efficient N-arylation of imidazole catalyzed by Cu(II) complexes with quaternary ammonium-functionalized 2-acetylpyridine acylhydrazone. *Polyhedron* **2019**, *165*, 22–30 DOI: 10.1016/J.POLY.2019.03.001.
- (6) Ziegler, T.; Rauk, A. On the calculation of bonding energies by the Hartree Fock Slater method. *Theor. Chim. Acta* **1977**, *46* (1), 1–10 DOI: 10.1007/BF02401406.
- (7) Ziegler, T.; Rauk, A. A theoretical study of the ethylene-metal bond in complexes between copper(1+), silver(1+), gold(1+), platinum(0) or platinum(2+) and ethylene, based on the Hartree-Fock-Slater transition-state method. *Inorg. Chem.* **1979**, *18* (6),

- 1
2
3 1558–1565 DOI: 10.1021/ic50196a034.
4
5
6
7 (8) Bickelhaupt, F. M.; Baerends, E. J. Kohn-Sham Density Functional Theory: Predicting
8 and Understanding Chemistry. In *Reviews in computational chemistry*; Lipkowitz, K. B.,
9 Boyd, D. B., Eds.; Wiley-VCH Verlag, 2000; Vol. 15, pp 1–86.
10
11
12
13
14 (9) Johnson, E. R.; Keinan, S.; Mori-Sánchez, P.; Contreras-García, J.; Cohen, A. J.; Yang,
15 W. Revealing Noncovalent Interactions. *J. Am. Chem. Soc.* **2010**, *132* (18), 6498–6506
16 DOI: 10.1021/ja100936w.
17
18
19
20
21
22 (10) Lefebvre, C.; Rubez, G.; Khartabil, H.; Boisson, J.-C.; Contreras-García, J.; Hénon, E.
23 Accurately extracting the signature of intermolecular interactions present in the NCI plot
24 of the reduced density gradient versus electron density. *Phys. Chem. Chem. Phys.* **2017**,
25 *19* (27), 17928–17936 DOI: 10.1039/C7CP02110K.
26
27
28
29
30
31
32 (11) Lefebvre, C.; Khartabil, H.; Boisson, J.-C.; Contreras-García, J.; Piquemal, J.-P.; Hénon,
33 E. The Independent Gradient Model: A New Approach for Probing Strong and Weak
34 Interactions in Molecules from Wave Function Calculations. *ChemPhysChem* **2018**, *19*
35 (6), 724–735 DOI: 10.1002/cphc.201701325.
36
37
38
39
40
41
42 (12) Bader, R. F. W. A quantum theory of molecular structure and its applications. *Chem. Rev.*
43 **1991**, *91* (5), 893–928 DOI: 10.1021/cr00005a013.
44
45
46
47
48 (13) Oxford Diffraction. Oxford Diffraction, CrysAlis PRO, Oxford Diffraction Ltd., Yarnton,
49 England, <https://www.rigaku.com/en/products/smc/crystalis> (accessed May 15, 2019).
50
51
52
53 (14) Altomare, A.; Cascarano, G.; Giacovazzo, C.; Guagliardi, A.; IUCr. Completion and
54
55
56
57
58
59
60

- 1
2
3 refinement of crystal structures with SIR 92. *J. Appl. Crystallogr.* **1993**, 26 (3), 343–350
4
5 DOI: 10.1107/S0021889892010331.
6
7
8
9 (15) Sheldrick, G. M.; IUCr. A short history of SHELX. *Acta Crystallogr. Sect. A Found.*
10
11 *Crystallogr.* **2008**, 64 (1), 112–122 DOI: 10.1107/S0108767307043930.
12
13
14 (16) Sheldrick, G. M.; IUCr. Crystal structure refinement with SHELXL. *Acta Crystallogr.*
15
16 *Sect. C Struct. Chem.* **2015**, 71 (1), 3–8 DOI: 10.1107/S2053229614024218.
17
18
19
20 (17) Farrugia, L. J.; IUCr. WinGX and ORTEP for Windows : an update. *J. Appl. Crystallogr.*
21
22 **2012**, 45 (4), 849–854 DOI: 10.1107/S0021889812029111.
23
24
25
26 (18) Macrae, C. F.; Edgington, P. R.; McCabe, P.; Pidcock, E.; Shields, G. P.; Taylor, R.;
27
28 Towler, M.; van de Streek, J.; IUCr. Mercury : visualization and analysis of crystal
29
30 structures. *J. Appl. Crystallogr.* **2006**, 39 (3), 453–457 DOI:
31
32 10.1107/S002188980600731X.
33
34
35
36 (19) Neese, F. The ORCA program system. *Wiley Interdiscip. Rev. Comput. Mol. Sci.* **2012**, 2
37
38 (1), 73–78 DOI: 10.1002/wcms.81.
39
40
41
42 (20) Neese, F. Software update: the ORCA program system, version 4.0. *Wiley Interdiscip.*
43
44 *Rev. Comput. Mol. Sci.* **2018**, 8 (1), e1327 DOI: 10.1002/wcms.1327.
45
46
47
48 (21) Zhang, Y.; Yang, W. Comment on “Generalized Gradient Approximation Made Simple.”
49
50 *Phys. Rev. Lett.* **1998**, 80 (4), 890–890 DOI: 10.1103/PhysRevLett.80.890.
51
52
53 (22) Grimme, S.; Antony, J.; Ehrlich, S.; Krieg, H. A consistent and accurate ab initio
54
55 parametrization of density functional dispersion correction (DFT-D) for the 94 elements
56
57
58
59
60

- 1
2
3 H-Pu. *J. Chem. Phys.* **2010**, *132* (15), 154104 DOI: 10.1063/1.3382344.
4
5
6
7 (23) Grimme, S.; Ehrlich, S.; Goerigk, L. Effect of the damping function in dispersion
8 corrected density functional theory. *J. Comput. Chem.* **2011**, *32* (7), 1456–1465 DOI:
9 10.1002/jcc.21759.
10
11
12
13
14 (24) Lenthe, E. van; Baerends, E. J.; Snijders, J. G. Relativistic regular two-component
15 Hamiltonians. *J. Chem. Phys.* **1993**, *99* (6), 4597–4610 DOI: 10.1063/1.466059.
16
17
18
19
20 (25) van Lenthe, E.; Baerends, E. J.; Snijders, J. G. Relativistic total energy using regular
21 approximations. *J. Chem. Phys.* **1994**, *101* (11), 9783–9792 DOI: 10.1063/1.467943.
22
23
24
25
26 (26) Wüllen, C. van. Molecular density functional calculations in the regular relativistic
27 approximation: Method, application to coinage metal diatomics, hydrides, fluorides and
28 chlorides, and comparison with first-order relativistic calculations. *J. Chem. Phys.* **1998**,
29 *109* (2), 392–399 DOI: 10.1063/1.476576.
30
31
32
33
34
35
36 (27) Pantazis, D. A.; Chen, X.-Y.; Landis, C. R.; Neese, F. All-Electron Scalar Relativistic
37 Basis Sets for Third-Row Transition Metal Atoms. *J. Chem. Theory Comput.* **2008**, *4* (6),
38 908–919 DOI: 10.1021/ct800047t.
39
40
41
42
43
44 (28) Pantazis, D. A.; Neese, F. All-Electron Scalar Relativistic Basis Sets for the Lanthanides.
45 *J. Chem. Theory Comput.* **2009**, *5* (9), 2229–2238 DOI: 10.1021/ct900090f.
46
47
48
49
50 (29) Weigend, F. Accurate Coulomb-fitting basis sets for H to Rn. *Phys. Chem. Chem. Phys.*
51 **2006**, *8* (9), 1057–1065 DOI: 10.1039/b515623h.
52
53
54
55 (30) Baerends, E. J.; Ziegler, T.; Atkins, A. J.; Autschbach, J.; Bashford, D.; Baseggio, O.;
56
57
58
59
60

- 1
2
3 Bérces, A.; Bickelhaupt, F. M.; Bo, C.; Boerritger, P. M.; et al. ADF2017, SCM,
4 Theoretical Chemistry, Vrije Universiteit, Amsterdam, The Netherlands,
5 <https://www.scm.com>.
6
7
8
9
10
11 (31) Fonseca Guerra, C.; Snijders, J. G.; te Velde, G.; Baerends, E. J. Towards an order- N
12 DFT method. *Theor. Chem. Accounts Theory, Comput. Model. (Theoretica Chim. Acta)*
13 **1998**, *99* (6), 391–403 DOI: 10.1007/s002140050353.
14
15
16
17
18
19 (32) te Velde, G.; Bickelhaupt, F. M.; van Gisbergen, S. J. A.; Guerra, C. F.; Baerends, E. J.;
20 Snijders, J. G.; Ziegler, T.; Fonseca Guerra, C.; van Gisbergen, S. J. A.; Snijders, J. G.; et
21 al. Chemistry with ADF. *J. Comput. Chem.* **2001**, *22* (9), 931–967 DOI: 10.1002/jcc.1056.
22
23
24
25
26
27 (33) Nalewajski, R. F.; Mrozek, J.; Mazur, G. Quantum chemical valence indices from the one-
28 determinantal difference approach. *Can. J. Chem.* **1996**, *74* (6), 1121–1130 DOI:
29 10.1139/v96-126.
30
31
32
33
34
35 (34) Mitoraj, M. P.; Michalak, A.; Ziegler, T. A Combined Charge and Energy Decomposition
36 Scheme for Bond Analysis. *J. Chem. Theory Comput.* **2009**, *5* (4), 962–975 DOI:
37 10.1021/ct800503d.
38
39
40
41
42
43 (35) Hirshfeld, F. L. Bonded-atom fragments for describing molecular charge densities. *Theor.*
44 *Chim. Acta* **1977**, *44* (2), 129–138 DOI: 10.1007/BF00549096.
45
46
47
48
49 (36) Becke, A. D. Density-functional exchange-energy approximation with correct asymptotic
50 behavior. *Phys. Rev. A* **1988**, *38* (6), 3098–3100 DOI: 10.1103/PhysRevA.38.3098.
51
52
53
54 (37) Perdew, J. P. Density-functional approximation for the correlation energy of the
55
56
57
58
59
60

- 1
2
3 inhomogeneous electron gas. *Phys. Rev. B* **1986**, *33* (12), 8822–8824 DOI:
4 10.1103/PhysRevB.33.8822.
5
6
7
8
9 (38) Perdew, J. P. Erratum: Density-functional approximation for the correlation energy of the
10 inhomogeneous electron gas. *Phys. Rev. B* **1986**, *34* (10), 7406–7406 DOI:
11 10.1103/PhysRevB.34.7406.
12
13
14
15
16 (39) Perdew, J. P.; Burke, K.; Ernzerhof, M. Generalized Gradient Approximation Made
17 Simple. *Phys. Rev. Lett.* **1996**, *77* (18), 3865–3868 DOI: 10.1103/PhysRevLett.77.3865.
18
19
20
21
22 (40) Zhao, Y.; Truhlar, D. G. A new local density functional for main-group thermochemistry,
23 transition metal bonding, thermochemical kinetics, and noncovalent interactions. *J. Chem.*
24 *Phys.* **2006**, *125* (19), 194101 DOI: 10.1063/1.2370993.
25
26
27
28
29
30 (41) Zhao, Y.; Truhlar, D. G. The M06 suite of density functionals for main group
31 thermochemistry, thermochemical kinetics, noncovalent interactions, excited states, and
32 transition elements: two new functionals and systematic testing of four M06-class
33 functionals and 12 other function. *Theor. Chem. Acc.* **2008**, *120* (1–3), 215–241 DOI:
34 10.1007/s00214-007-0310-x.
35
36
37
38
39
40
41
42 (42) Lu, T.; Chen, F. Multiwfn: A multifunctional wavefunction analyzer. *J. Comput. Chem.*
43 **2012**, *33* (5), 580–592 DOI: 10.1002/jcc.22885.
44
45
46
47
48 (43) Hujo, W.; Grimme, S. Performance of the van der Waals Density Functional VV10 and
49 (hybrid)GGA Variants for Thermochemistry and Noncovalent Interactions. *J. Chem.*
50 *Theory Comput.* **2011**, *7* (12), 3866–3871 DOI: 10.1021/ct200644w.
51
52
53
54
55
56
57
58
59
60

- 1
2
3 (44) Vydrov, O. A.; Van Voorhis, T. Nonlocal van der Waals density functional: the simpler
4 the better. *J. Chem. Phys.* **2010**, *133* (24), 244103 DOI: 10.1063/1.3521275.
5
6
7
8
9 (45) Chumakov, Y. M.; Tsapkov, V. I.; Antosyak, B. Y.; Bairac, N. N.; Simonov, Y. A.;
10 Bocelli, G.; Pahontu, E.; Gulea, A. P. Crystal structures of copper(II) nitrate, copper(II)
11 chloride, and copper(II) perchlorate complexes with 2-formylpyridine semicarbazone.
12 *Crystallogr. Reports* **2009**, *54* (3), 455–463 DOI: 10.1134/S1063774509030146.
13
14
15
16
17
18
19 (46) Sangeetha, N. R.; Pal, S.; Anson, C. E.; Powell, A. K.; Pal, S. A one-dimensional
20 assembly of copper(II) polyhedra via dual use of hydrogen-bonding and π - π interaction.
21 *Inorg. Chem. Commun.* **2000**, *3* (8), 415–419 DOI: 10.1016/S1387-7003(00)00103-9.
22
23
24
25
26
27 (47) Despaigne, A. A. R.; Silva, J. G. da; Carmo, A. C. M. do; Sives, F.; Piro, O. E.;
28 Castellano, E. E.; Beraldo, H. Copper(II) and zinc(II) complexes with 2-formylpyridine-
29 derived hydrazones. *Polyhedron* **2009**, *28* (17), 3797–3803 DOI:
30 10.1016/J.POLY.2009.07.059.
31
32
33
34
35
36
37 (48) Datta, A.; Das, K.; Jhou, Y.-M.; Huang, J.-H.; Lee, H. M.; IUCr. Dichlorido{ N '-[1-(2-
38 pyridin-2-yl)ethylidene]acetohydrazide- κ 2 N ', O }copper(II). *Acta Crystallogr. Sect. E*
39 *Struct. Reports Online* **2011**, *67* (1), m123–m123 DOI: 10.1107/S1600536810053195.
40
41
42
43
44
45 (49) Datta, A.; Sheu, S.-C.; Liu, P.-H.; Huang, J.-H.; IUCr. Dichlorido{ N '-[(pyridin-2-
46 yl)methylidene- κ N]acetohydrazide- κ 2 N ', O }copper(II). *Acta Crystallogr. Sect. E*
47 *Struct. Reports Online* **2011**, *67* (12), m1852–m1852 DOI: 10.1107/S1600536811049671.
48
49
50
51
52
53 (50) Shaabani, B.; Khandar, A. A.; Mahmoudi, F.; Maestro, M. A.; Balula, S. S.; Cunha-Silva,
54 L. Novel binuclear Cu(II) complexes combining a semicarbazone Schiff base with distinct
55
56
57
58
59
60

- 1
2
3 bridging ligands: Structure and antimicrobial activity. *Polyhedron* **2013**, *57*, 118–126
4
5 DOI: 10.1016/J.POLY.2013.04.016.
6
7
8
9 (51) Fousiamol, M. M.; Sithambaresan, M.; Smolenski, V. A.; Jasinski, J. P.; Kurup, M. R. P.
10 Halogen/azide bridged box dimer copper(II) complexes of 2-benzoylpyridine-3-
11 methoxybenzhydrazone: Structural and spectral studies. *Polyhedron* **2018**, *141*, 60–68
12
13 DOI: 10.1016/J.POLY.2017.11.024.
14
15
16
17
18 (52) Leovac, V. M.; Rodić, M. V.; Jovanović, L. S.; Joksović, M. D.; Stanojković, T.; Vujčić,
19 M.; Sladić, D.; Marković, V.; Vojinović-Ješić, L. S. Transition Metal Complexes with 1-
20 Adamantoyl Hydrazones - Cytotoxic Copper(II) Complexes of Tri- and Tetradentate
21
22 Pyridine Chelators Containing an Adamantane Ring System. *Eur. J. Inorg. Chem.* **2015**,
23
24 *2015* (5), 882–895 DOI: 10.1002/ejic.201403050.
25
26
27
28
29
30
31 (53) Yang, L.; Powell, D. R.; Houser, R. P. Structural variation in copper(i) complexes with
32
33 pyridylmethanamide ligands: structural analysis with a new four-coordinate geometry
34
35 index, τ 4. *Dalt. Trans.* **2007**, No. 9, 955–964 DOI: 10.1039/B617136B.
36
37
38
39 (54) Addison, A. W.; Rao, T. N.; Reedijk, J.; van Rijn, J.; Verschoor, G. C. Synthesis,
40
41 structure, and spectroscopic properties of copper(II) compounds containing nitrogen–
42
43 sulphur donor ligands; the crystal and molecular structure of aqua[1,7-bis(N-
44
45 methylbenzimidazol-2'-yl)-2,6-dithiaheptane]copper(II) perchlorate. *J. Chem. Soc., Dalt.*
46
47 *Trans.* **1984**, No. 7, 1349–1356 DOI: 10.1039/DT9840001349.
48
49
50
51 (55) Zlatar, M.; Allan, M.; Fedor, J. Excited states of Pt(PF₃)₃ and their
52
53 role in focused electron beam nanofabrication. *J. Phys. Chem. C* **2016**, *120* (19), 10667–
54
55
56
57
58
59
60

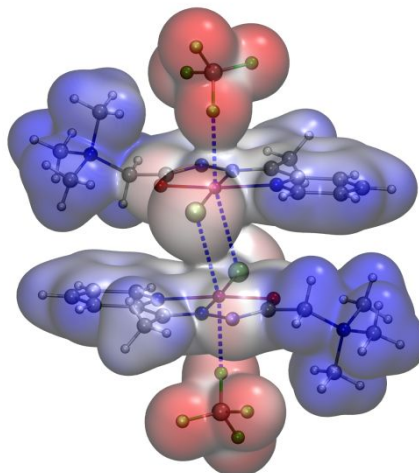
1
2
3 10674 DOI: 10.1021/acs.jpcc.6b02660.
4
5

6 (56) Caldeweyher, E.; Bannwarth, C.; Grimme, S. Extension of the D3 dispersion coefficient
7 model. *J. Chem. Phys.* **2017**, *147* (3), 034112 DOI: 10.1063/1.4993215.
8
9

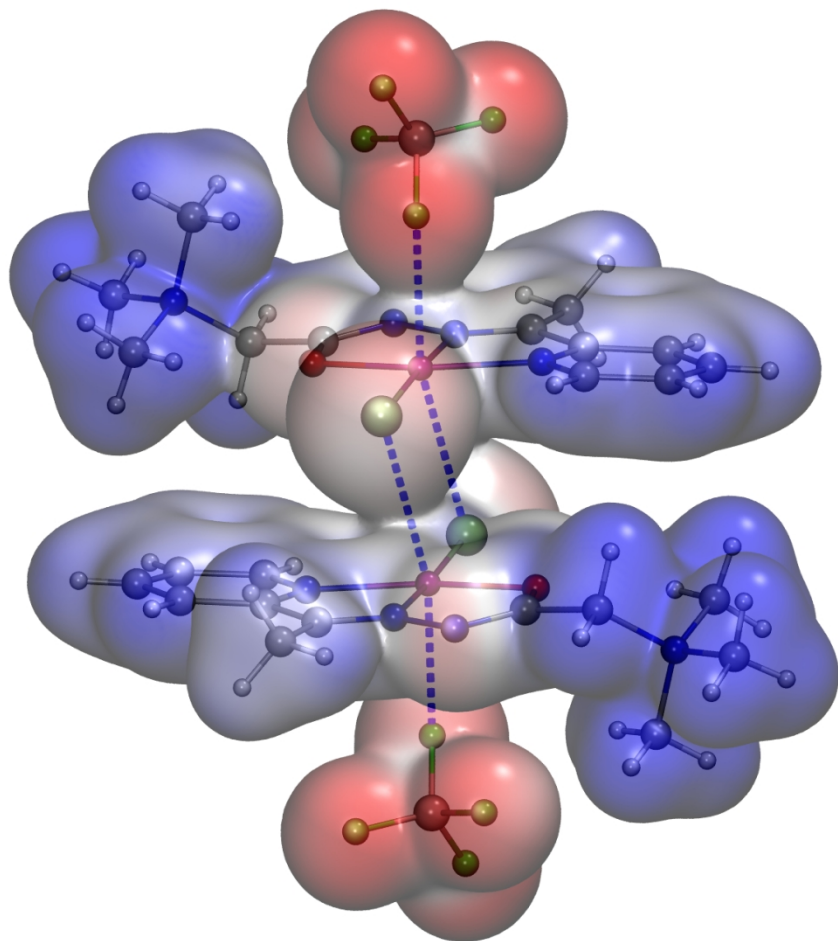
10
11
12 (57) Horn, P. R.; Mao, Y.; Head-Gordon, M. Defining the contributions of permanent
13 electrostatics, Pauli repulsion, and dispersion in density functional theory calculations of
14 intermolecular interaction energies. *J. Chem. Phys.* **2016**, *144* (11), 114107 DOI:
15
16
17 10.1063/1.4942921.
18
19
20
21
22
23
24
25
26
27
28
29
30
31
32
33
34
35
36
37
38
39
40
41
42
43
44
45
46
47
48
49
50
51
52
53
54
55
56
57
58
59
60

1
2
3 **SYNOPSIS:** Are BF_4^- , NO_3^- and ClO_4^- coordinatively or electrostatically bonded to Cu(II) ?

4
5 The synergy between the crystal structure determination and computational chemistry allows
6
7 identification of all interactions present in crystals and answer questions whether weakly
8
9 coordinated anions belong to the inner or outer sphere of the complex.
10
11
12
13
14



1
2
3
4
5
6
7
8
9
10
11
12
13
14
15
16
17
18
19
20
21
22
23
24
25
26
27
28
29
30
31
32
33
34
35
36
37
38
39
40
41
42
43
44
45
46
47
48
49
50
51
52
53
54
55
56
57
58
59
60



Graphical Abstract

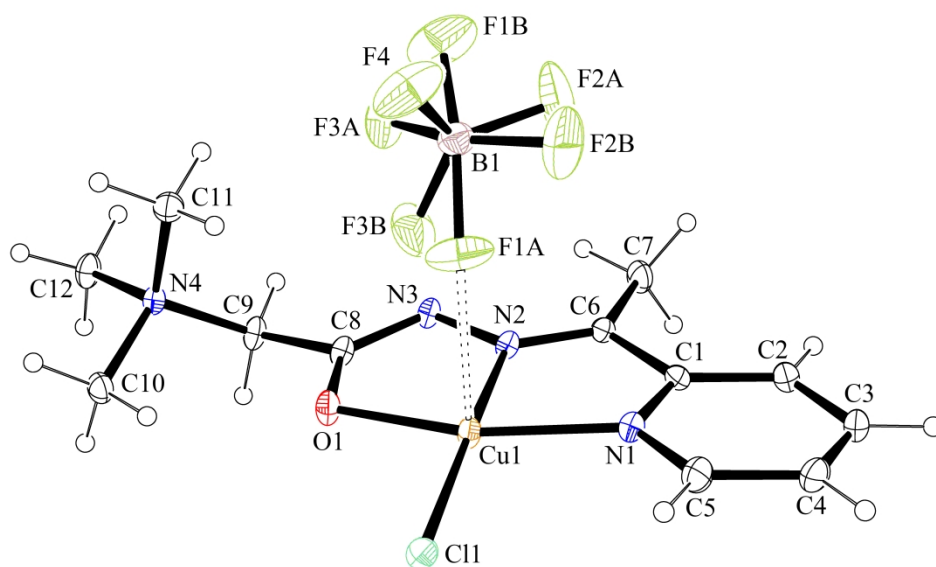


Figure 1. a) ORTEP presentation of the [CuLCl]BF₄ (1). Thermal ellipsoids are drawn at the 30% probability level. Long contact Cu--F is represented as a dashed line.

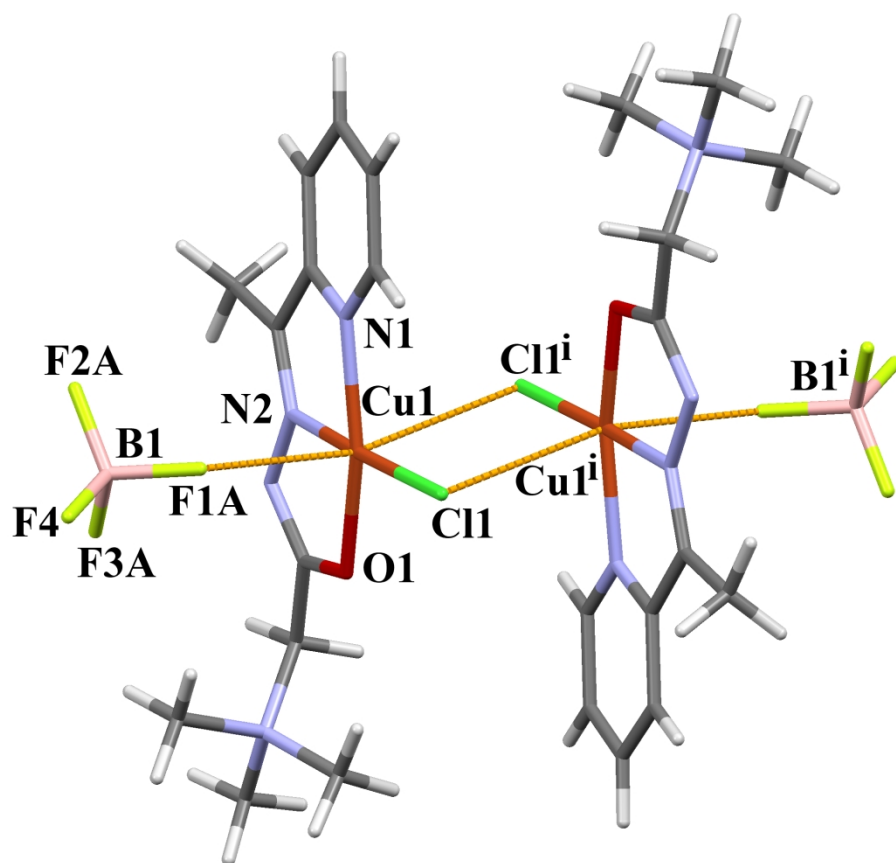


Figure 1b) View of the dimeric unit of 1 of pseudo-octahedral geometry

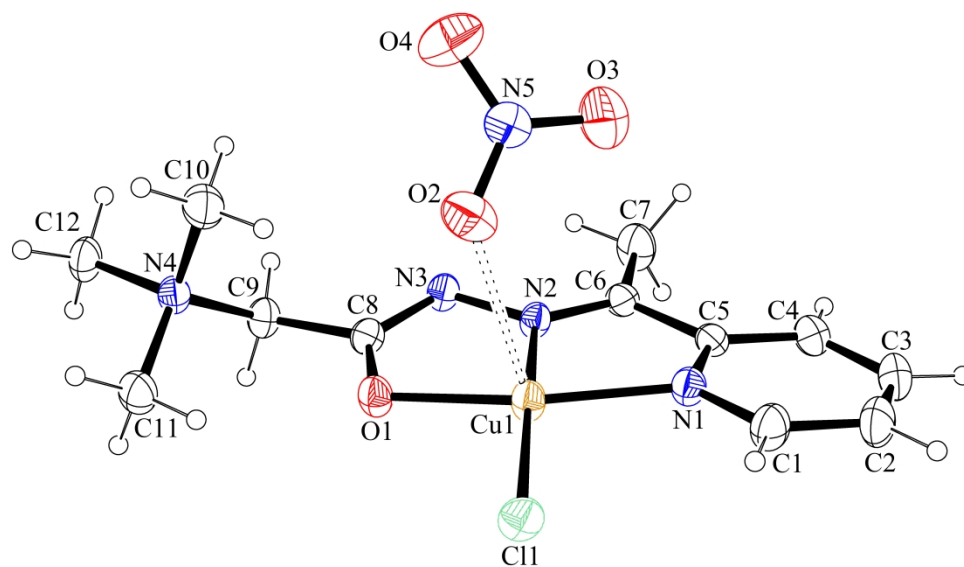


Figure 2. ORTEP presentation of the [CuLCl]NO₃ (2). Thermal ellipsoids are drawn at the 30% probability level. Long contact C--O is represented as a dashed line

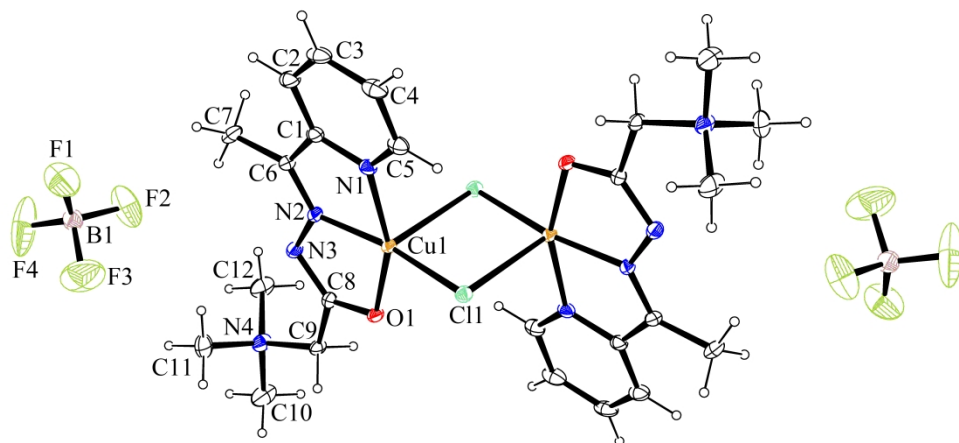


Figure 3. ORTEP presentation of the [Cu₂L₂Cl₂](BF₄)₂ (3)

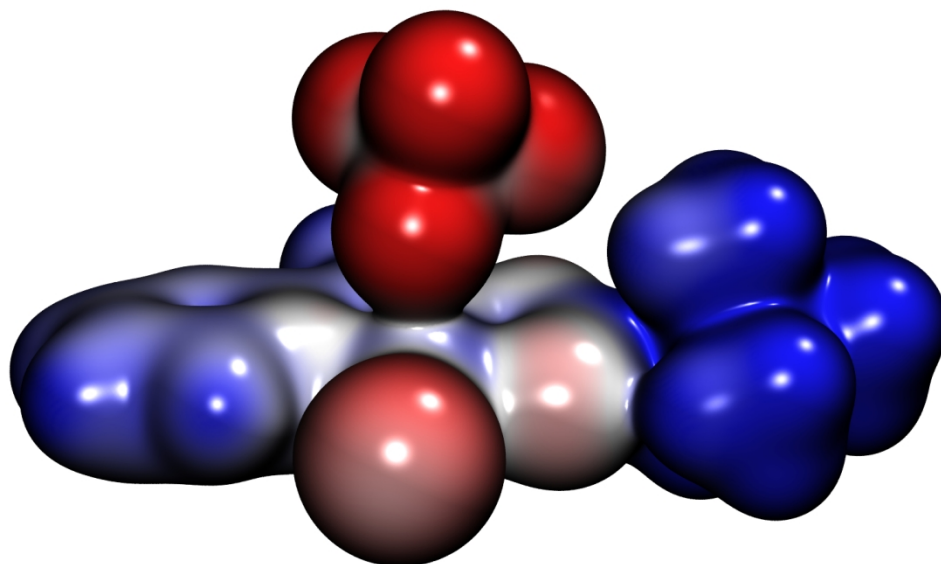


Figure 4a. Electrostatic potential surface of 1

1
2
3
4
5
6
7
8
9
10
11
12
13
14
15
16
17
18
19
20
21
22
23
24
25
26
27
28
29
30
31
32
33
34
35
36
37
38
39
40
41
42
43
44
45
46
47
48
49
50
51
52
53
54
55
56
57
58
59
60

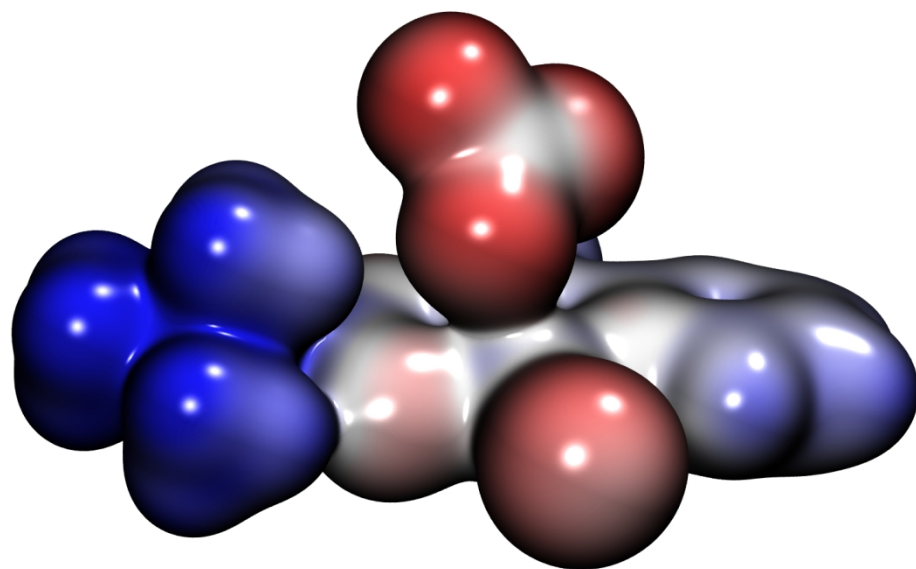


Figure 4b. Electrostatic potential surface of 2

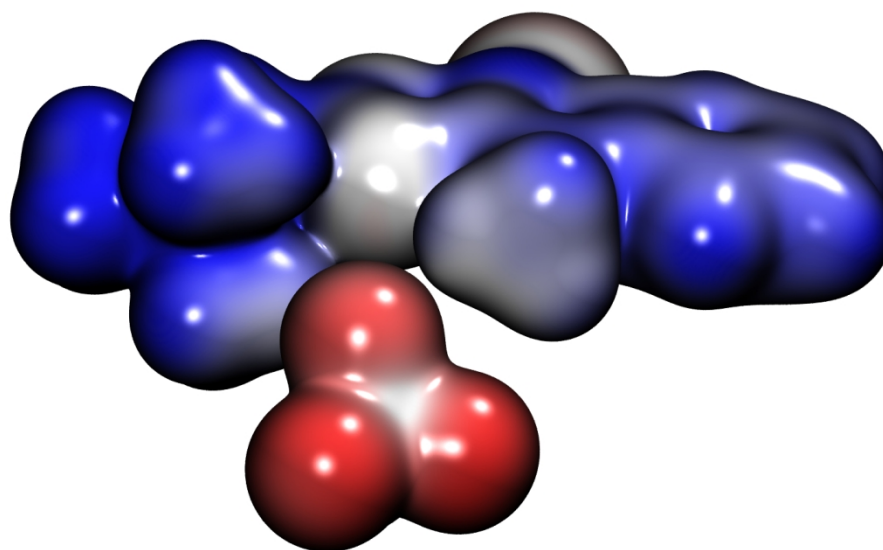


Figure 4c. Electrostatic potential surface of 3

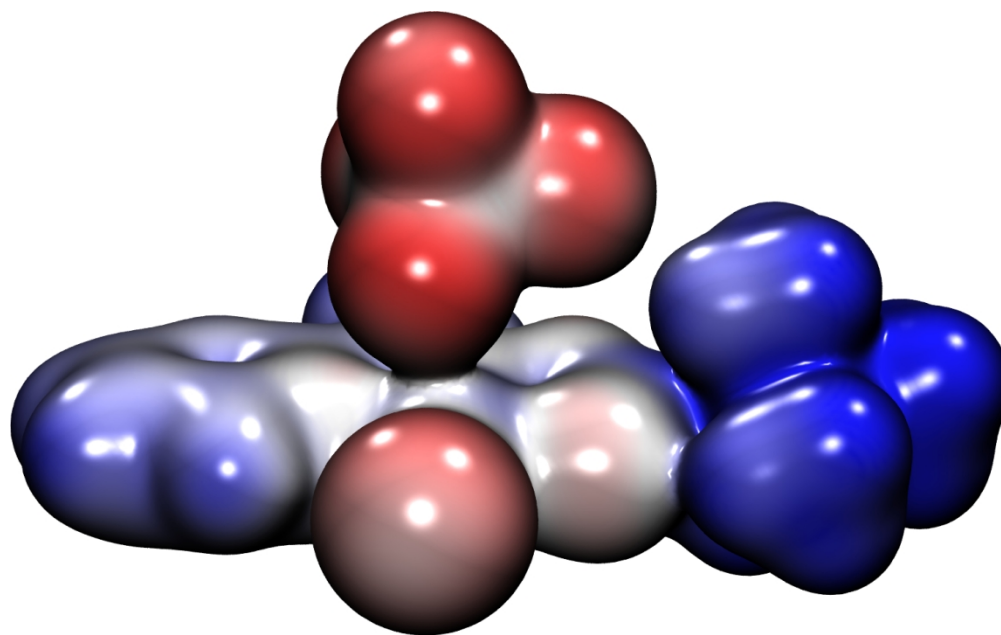


Figure 4d. Electrostatic potential surface for 4--ClO₄⁻

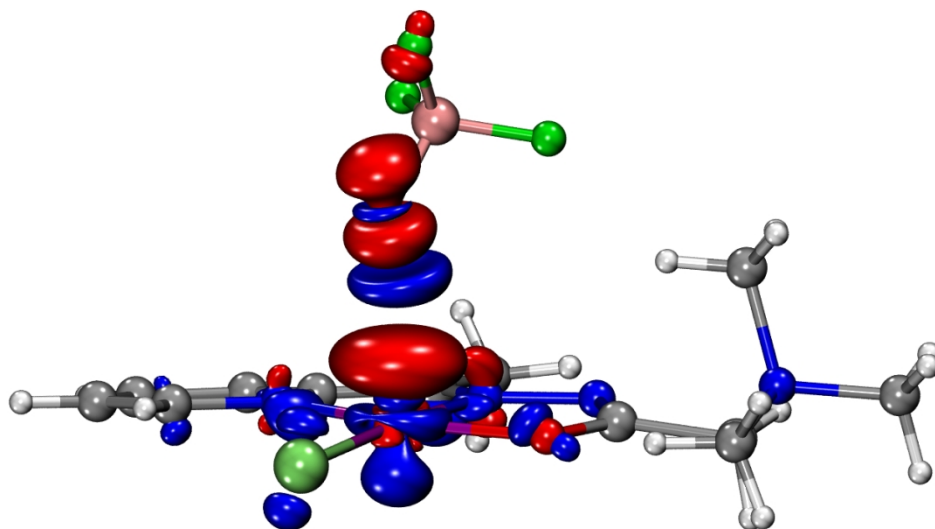


Figure 5a. Covalent deformation density channels from NOCV analysis for 1 (metal-ligand)

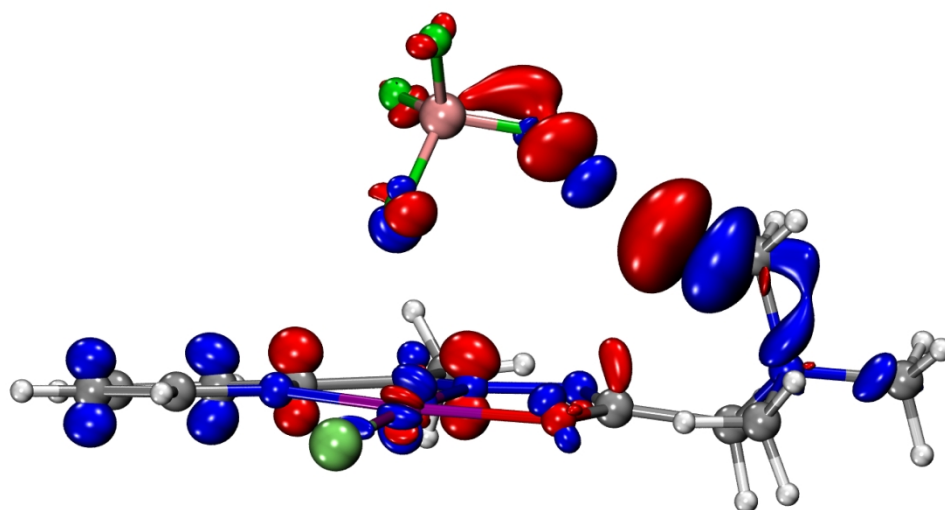


Figure 5b. Covalent deformation density channels from NOCV analysis for 1 (hydrogen bond)

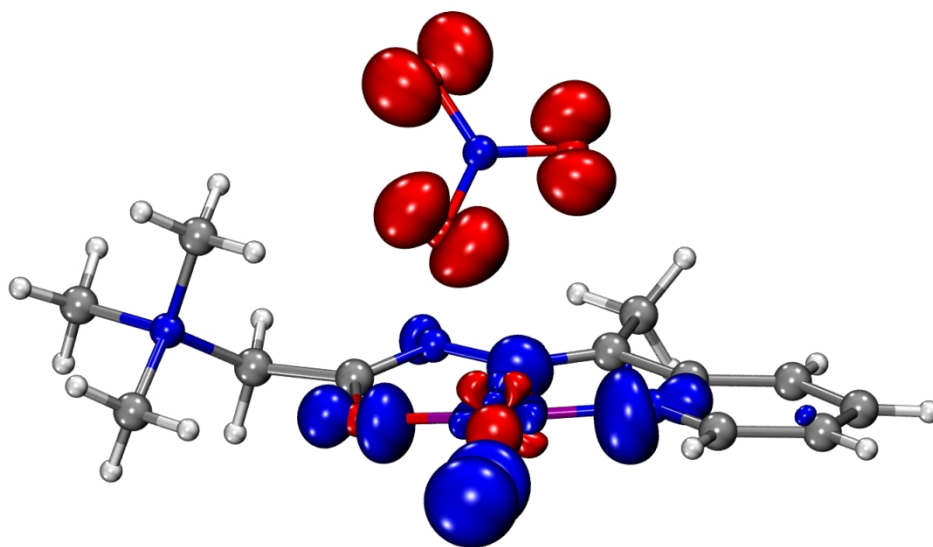


Figure 5c. Covalent deformation density channels from NOCV analysis for 2 (metal-ligand)

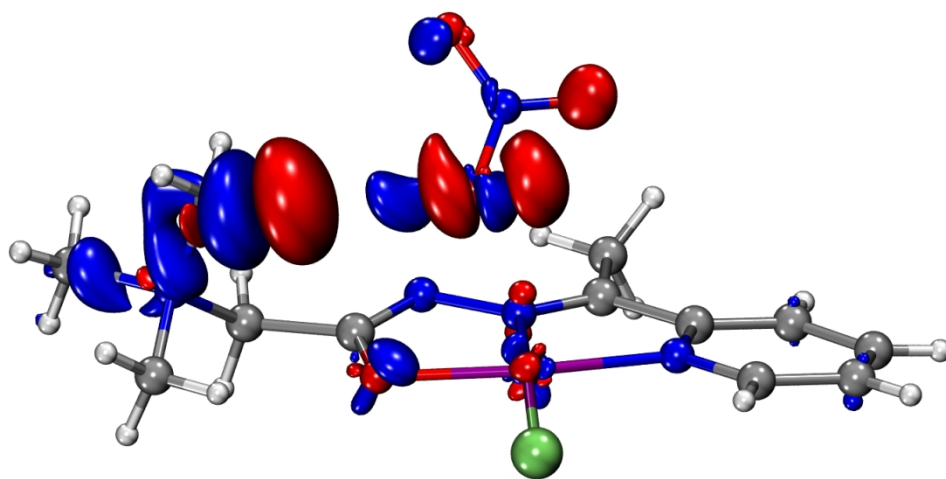


Figure 5d. Covalent deformation density channels from NOCV analysis for 2 (hydrogen bond)

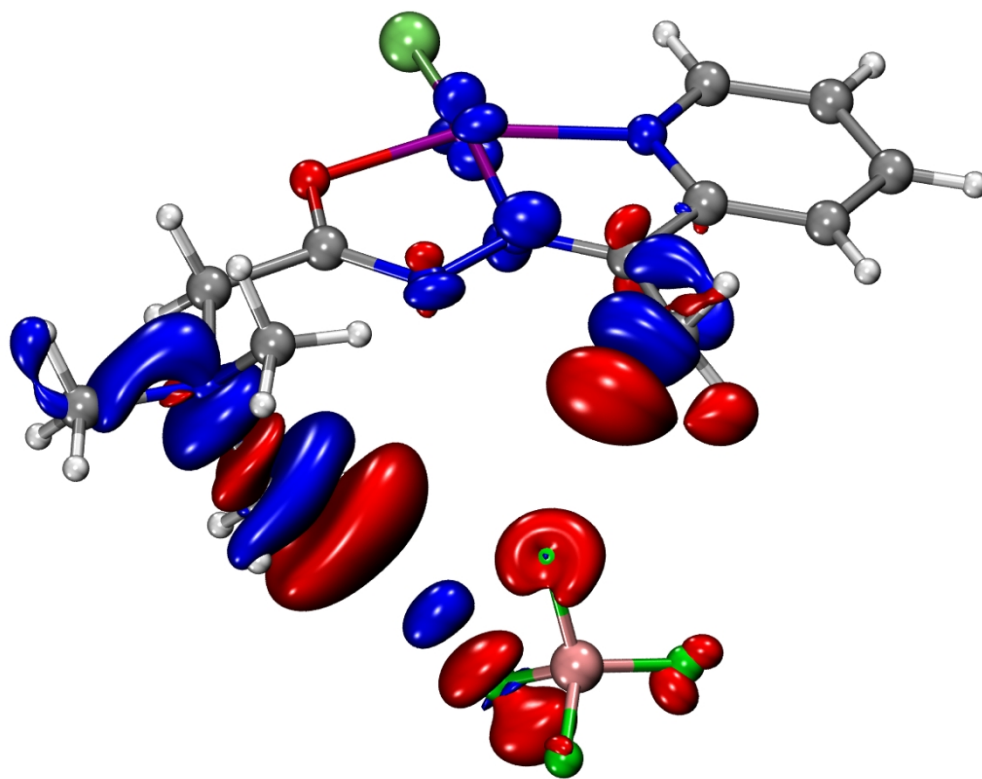


Figure 5e. Covalent deformation density channels from NOCV analysis for 3 (hydrogen bond 1)

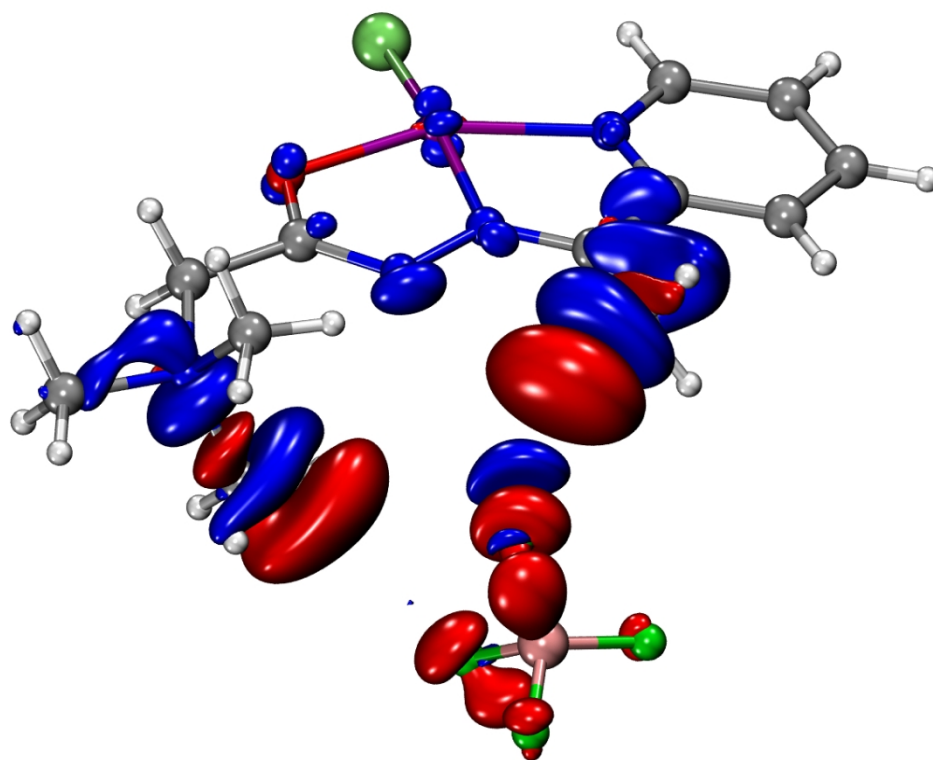


Figure 5f. Covalent deformation density channels from NOCV analysis for 3 (hydrogen bond 2)

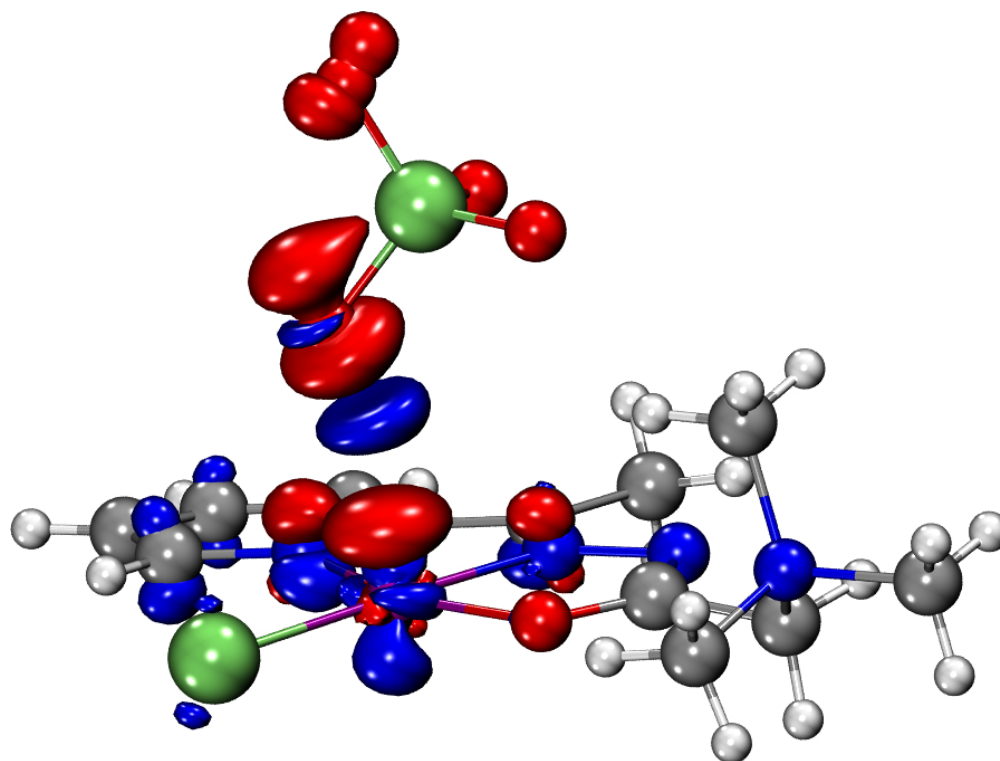


Figure 5g. Covalent deformation density channels from NOCV analysis for 4 (metal-ligand)

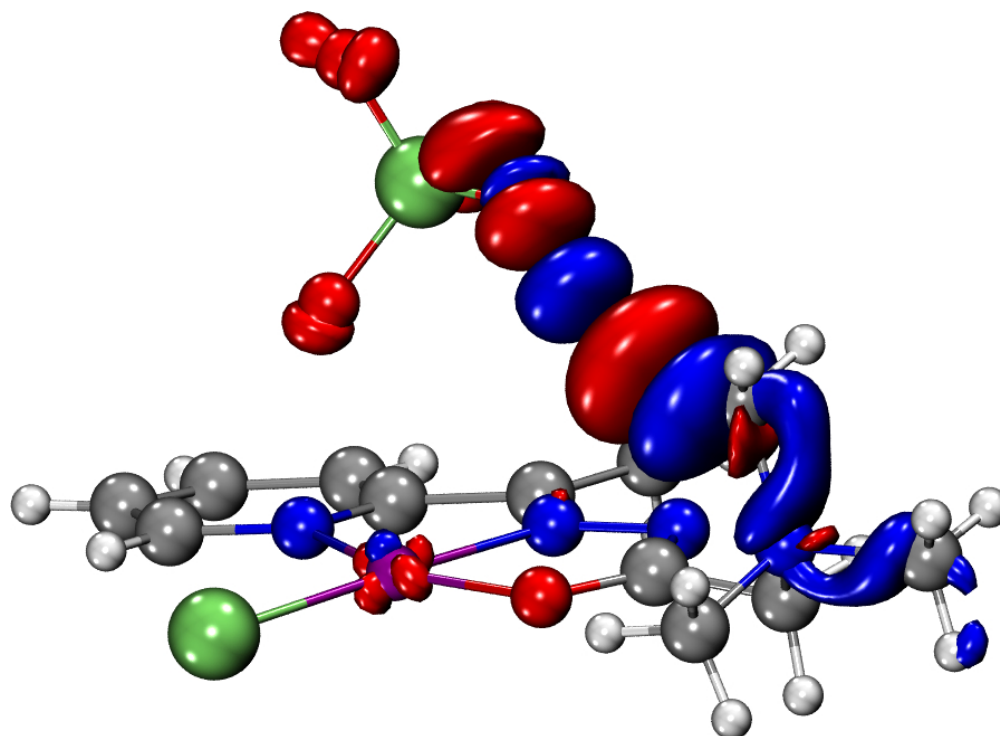


Figure 5h. Covalent deformation density channels from NOCV analysis for 4 (hydrogen-bond)

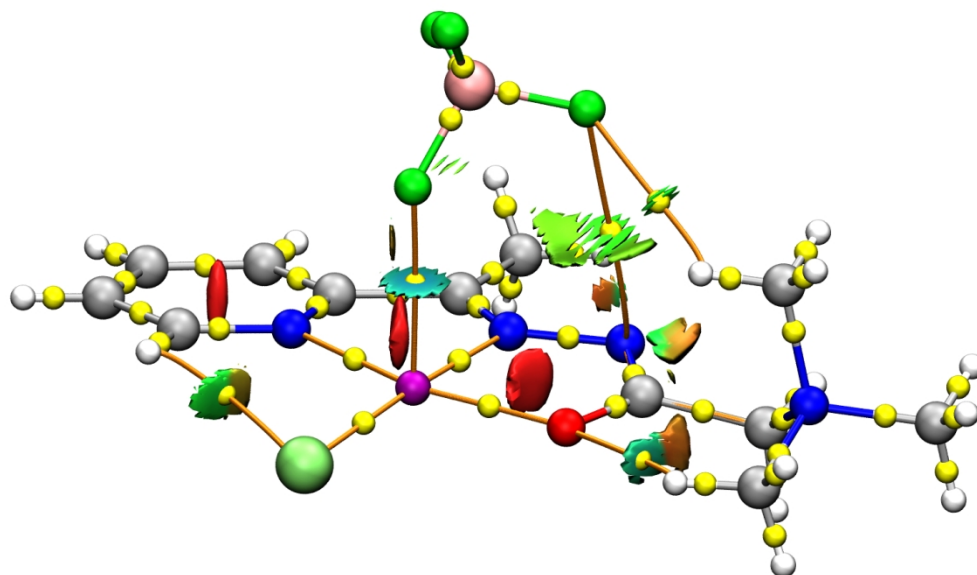


Figure 6a. NCI plots for 1

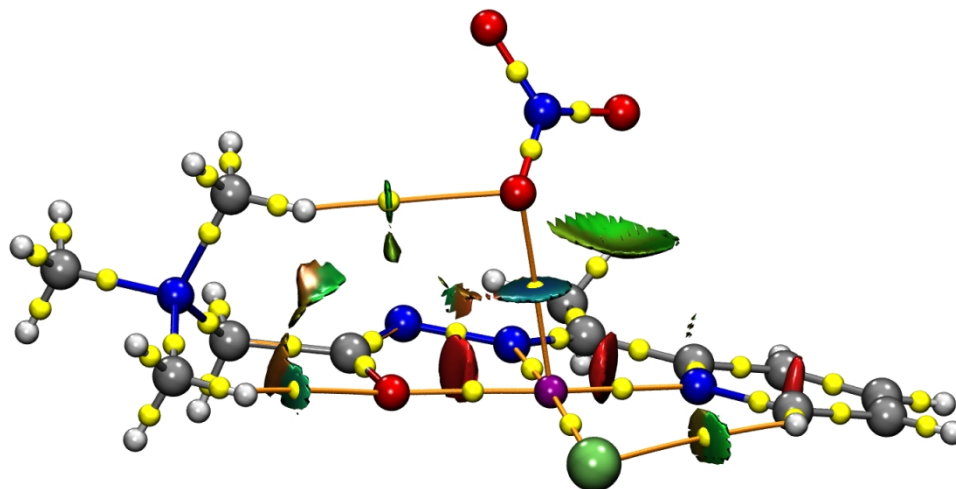


Figure 6b. NCI plots for 2

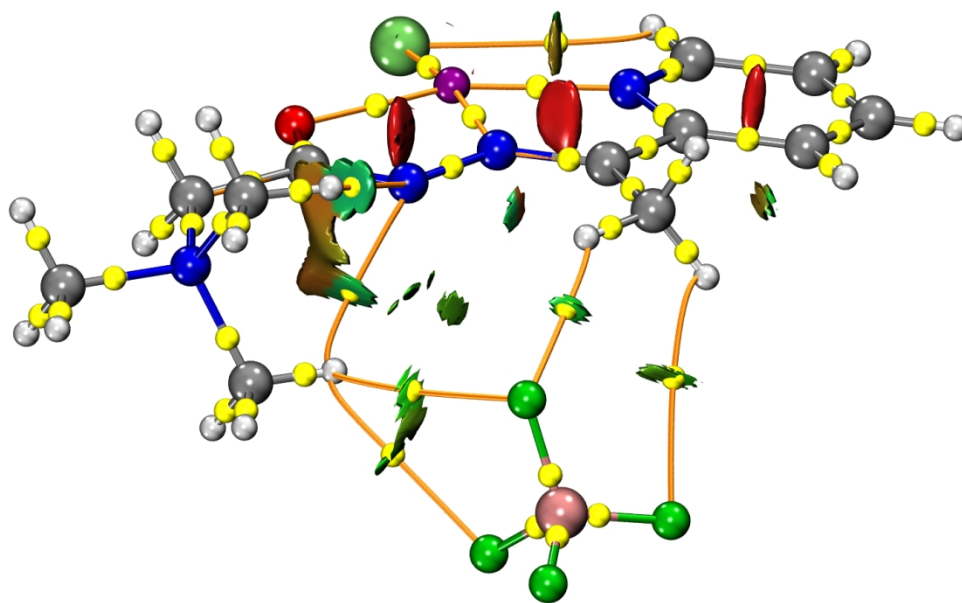


Figure 6c. NCI plots for 3

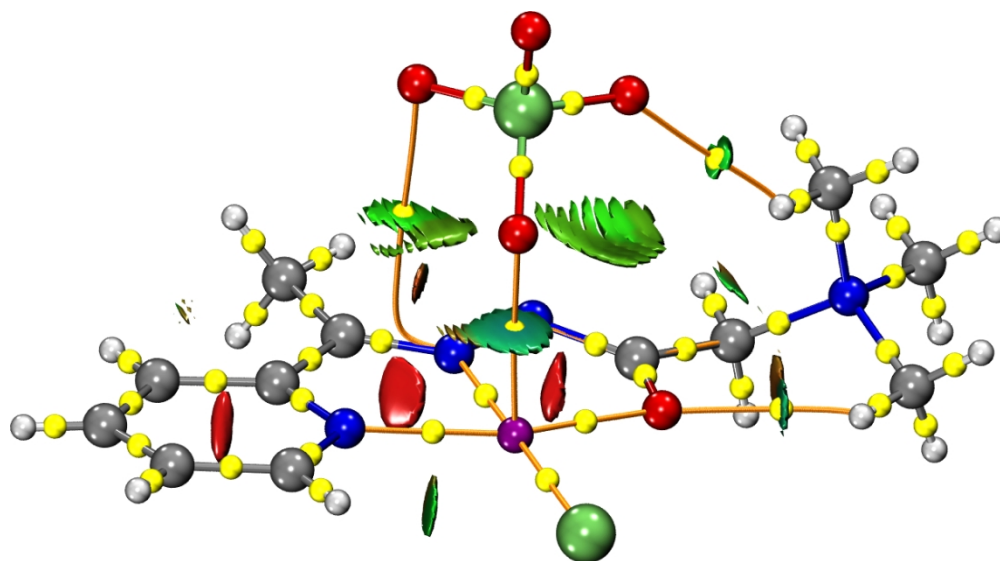


Figure 6d. NCI plots for 4

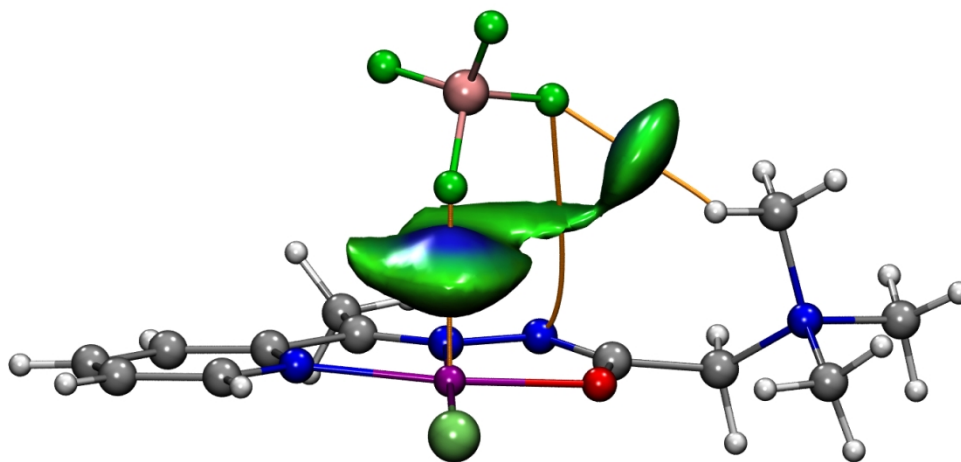


Figure 7a. IGM plots for 1

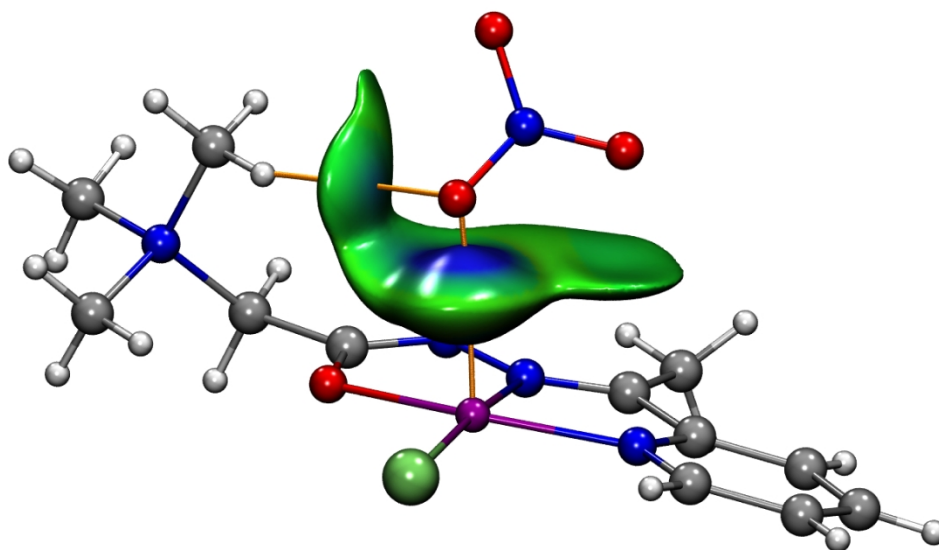


Figure 7b. IGM plots for 2

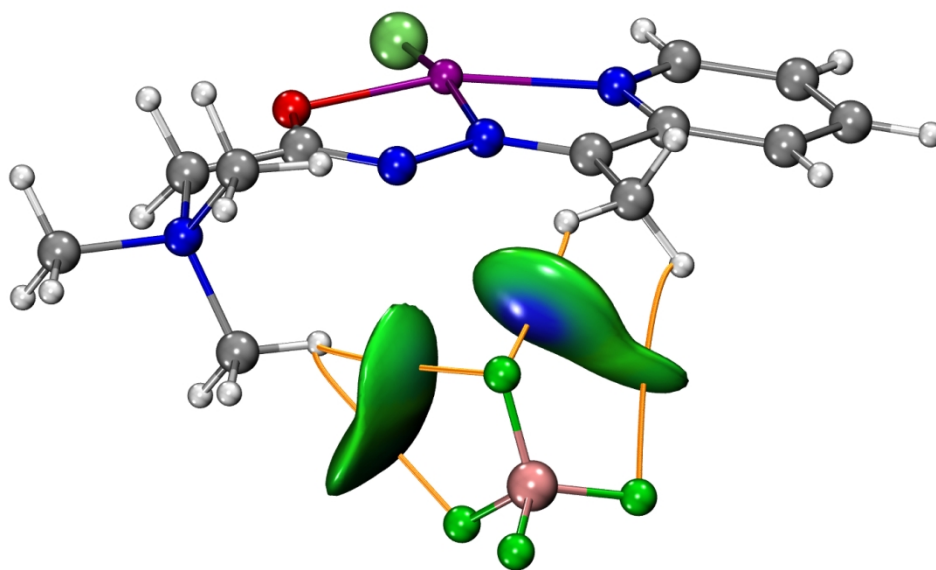


Figure 7c. IGM plots for 3

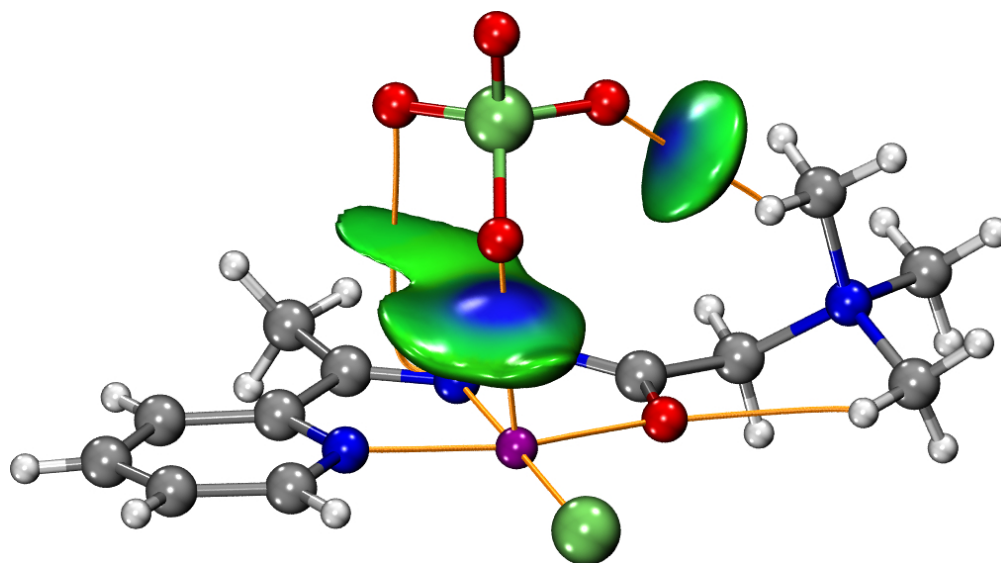


Figure 7d. IGM plots for 4

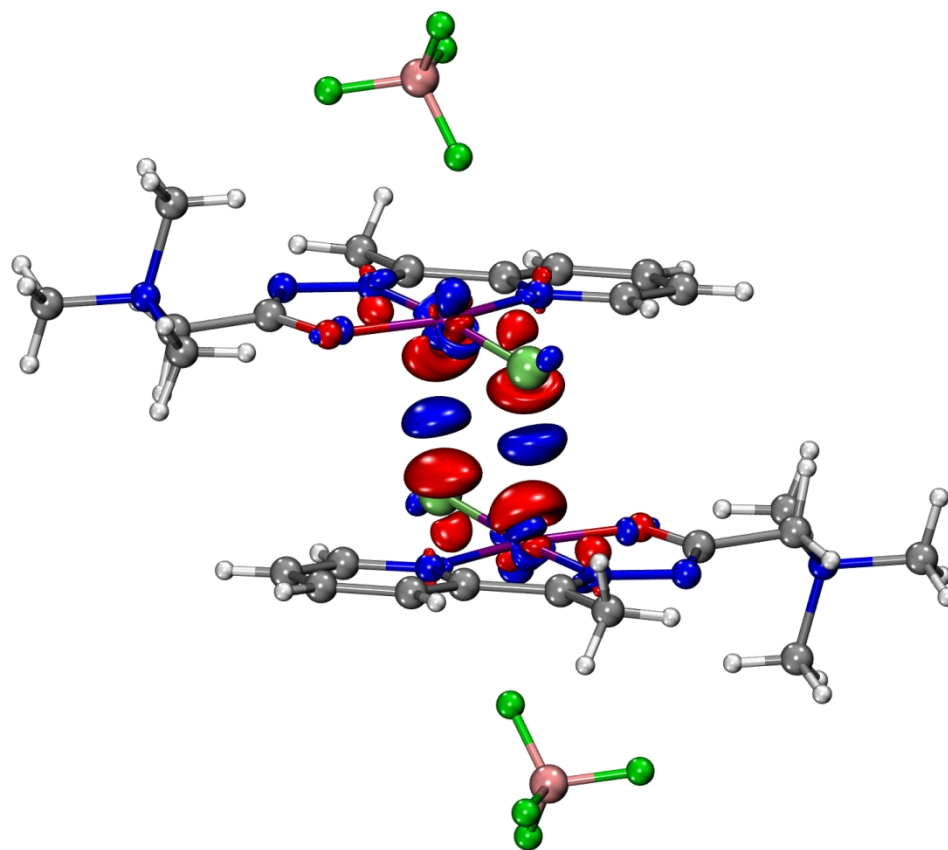


Figure 8a. Covalent deformation density channels from NOCV analysis for 1--1

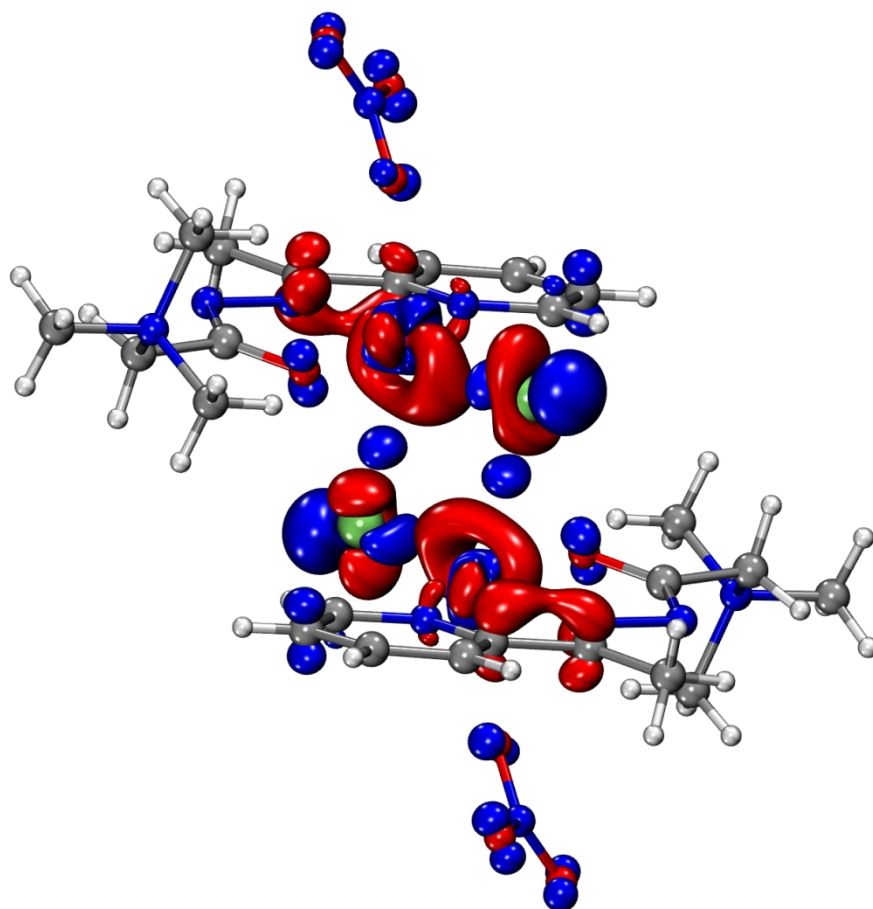


Figure 8b. Covalent deformation density channels from NOCV analysis for 2--2

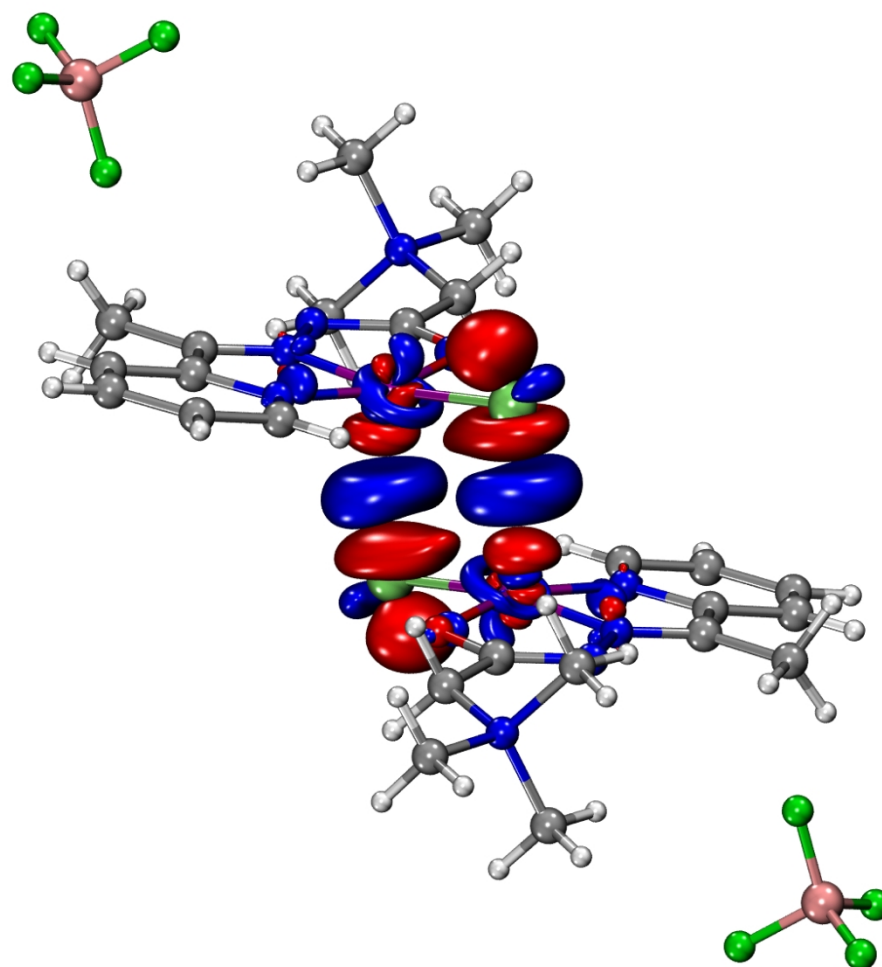


Figure 8c. Covalent deformation density channels from NOCV analysis for 3--3

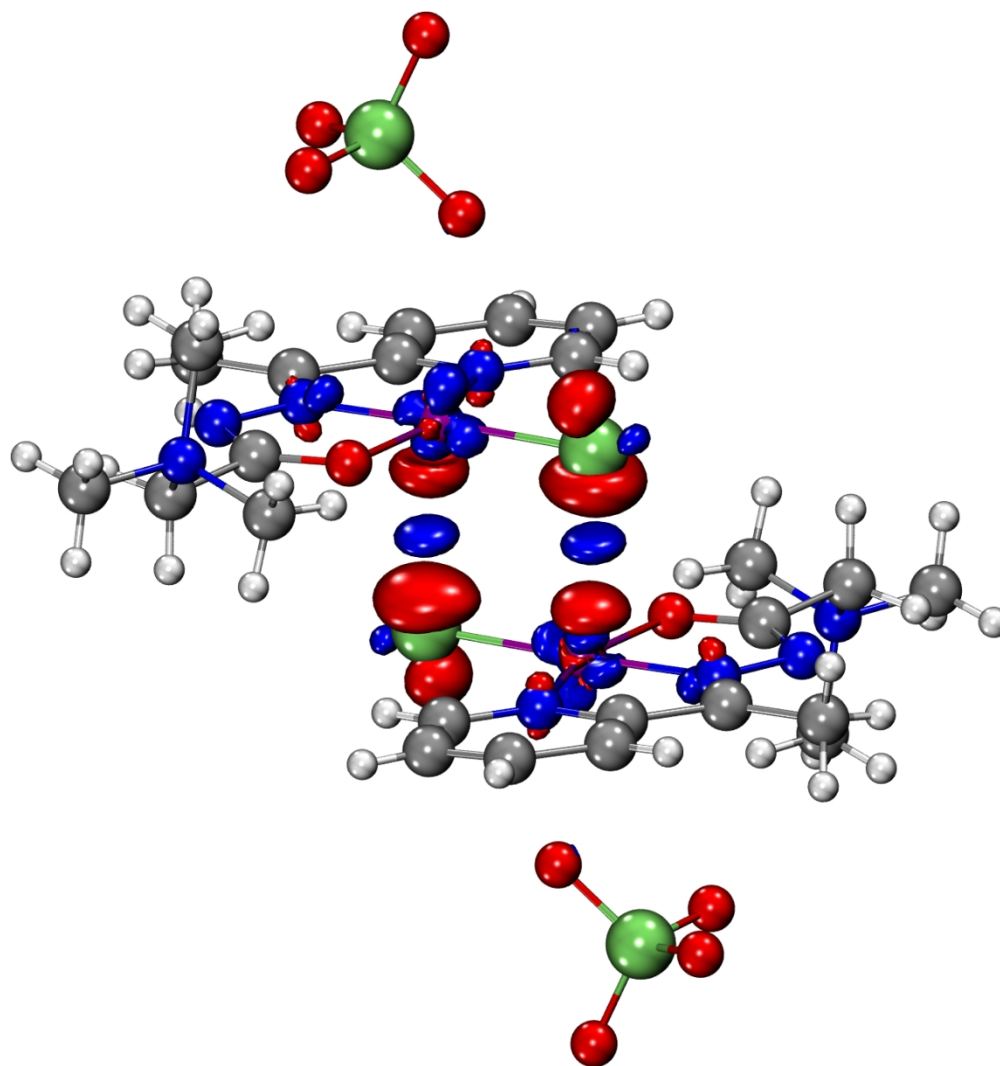


Figure 8d. Covalent deformation density channels from NOCV analysis for 4--4

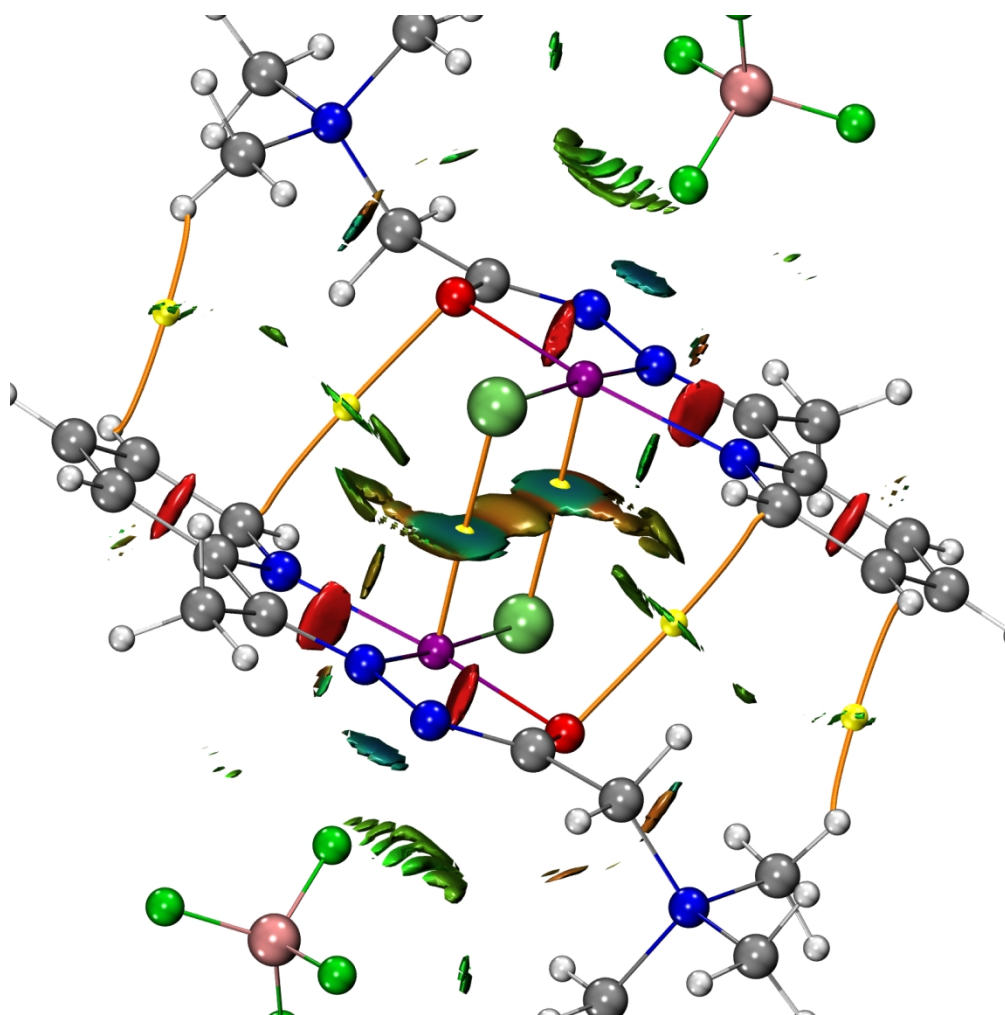


Figure 9a. NCI plots for 1--1

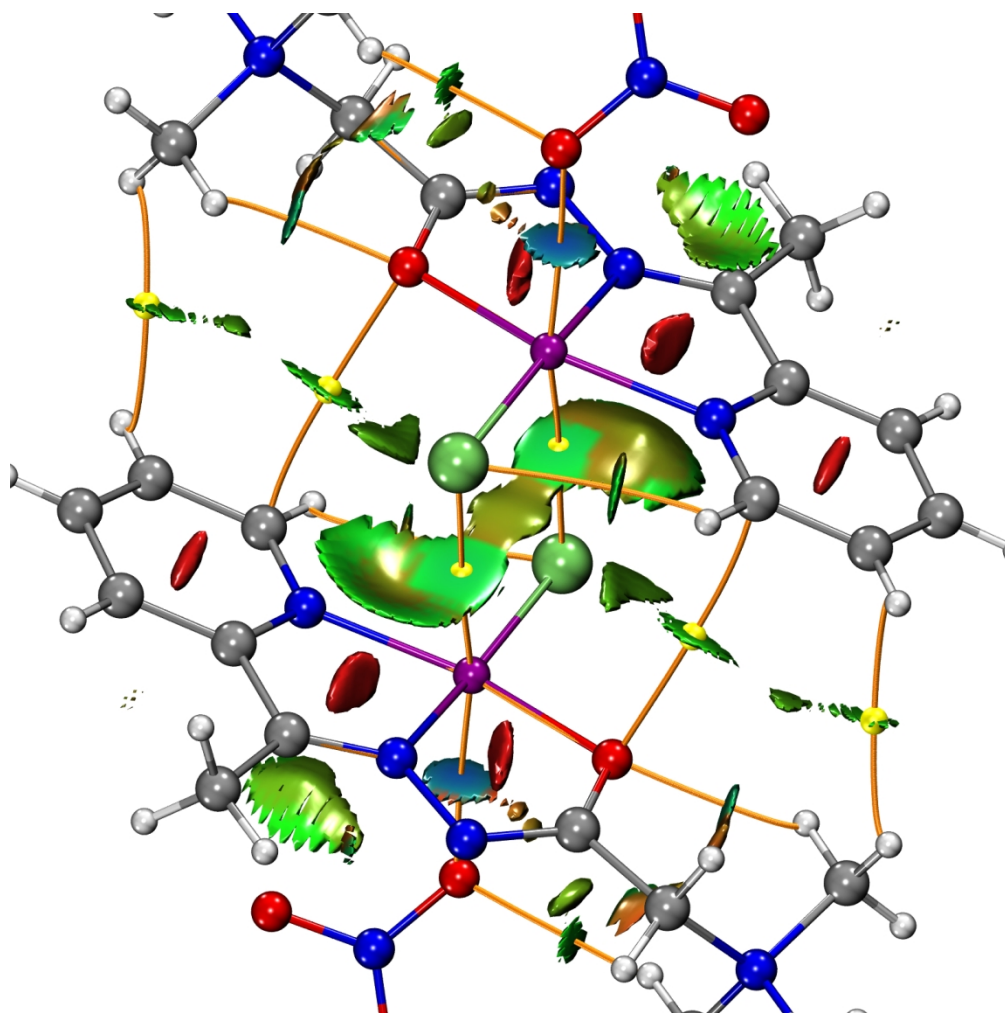


Figure 9b. NCI plots for 2--2

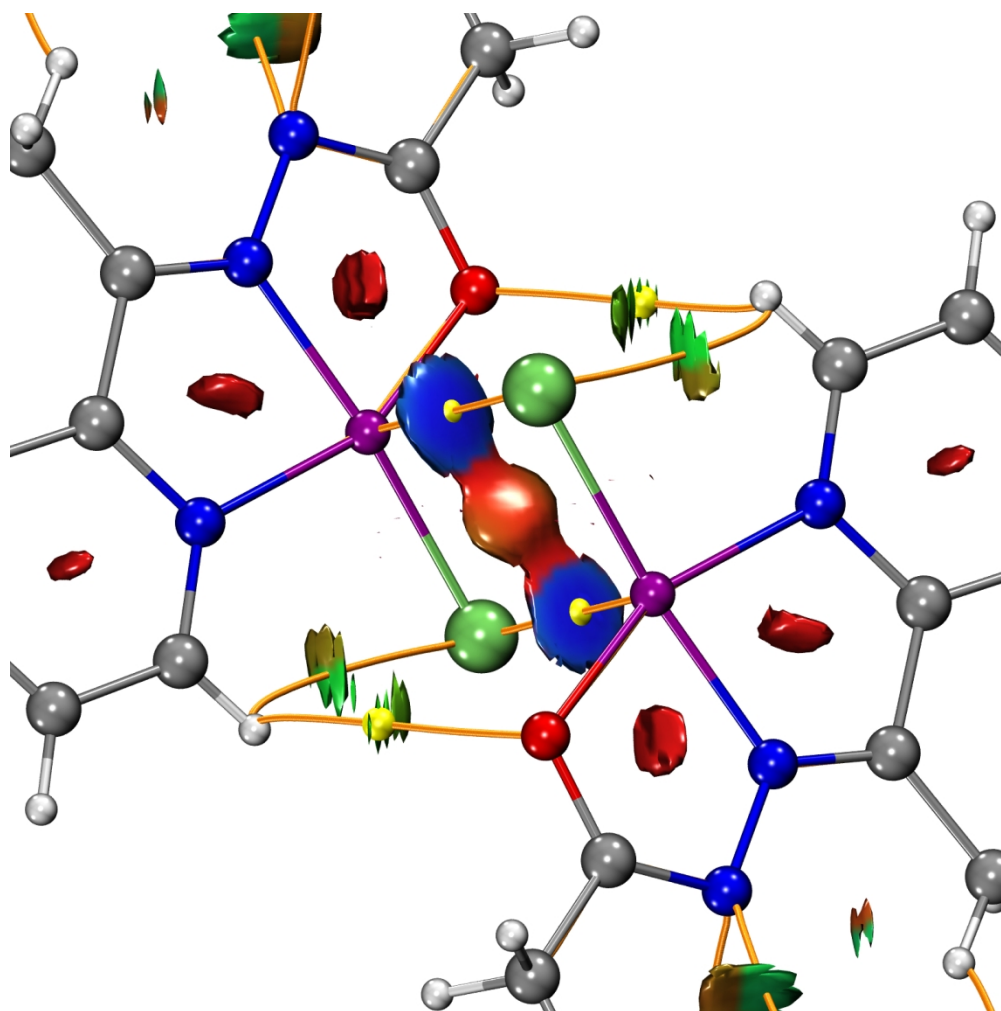


Figure 9c. NCI plots for 3--3

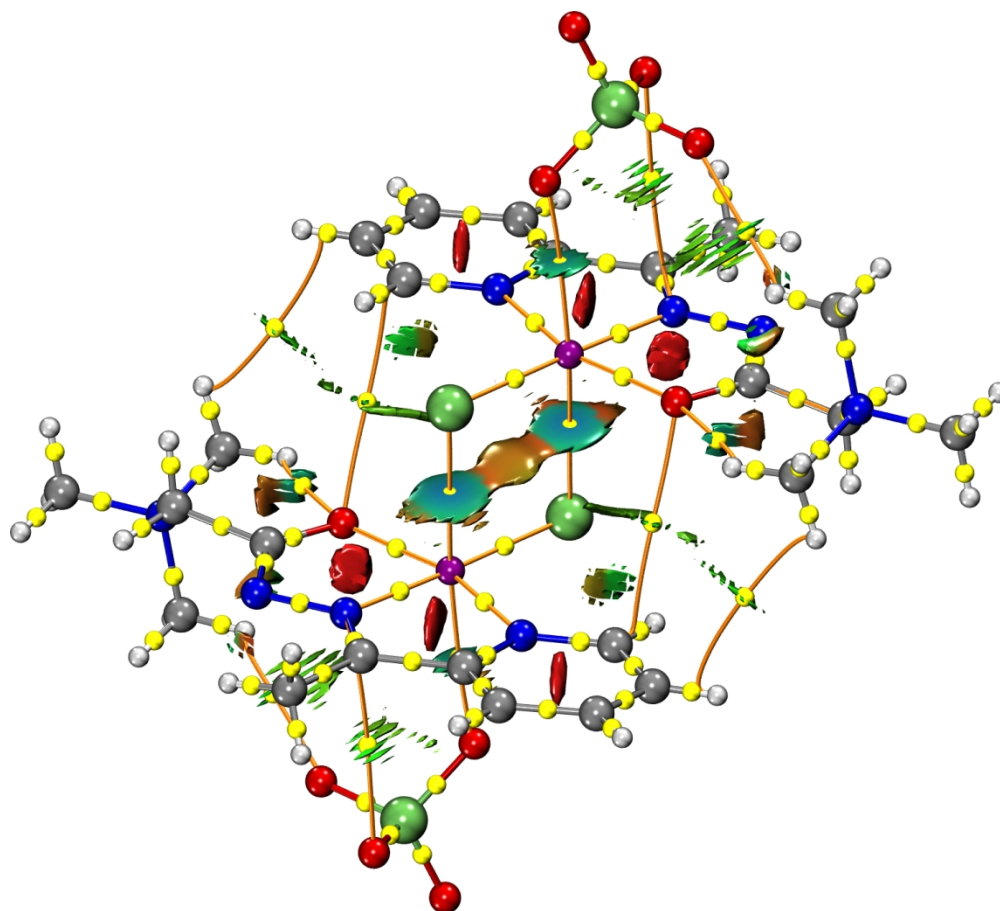


Figure 9d. NCI plot for 4--4

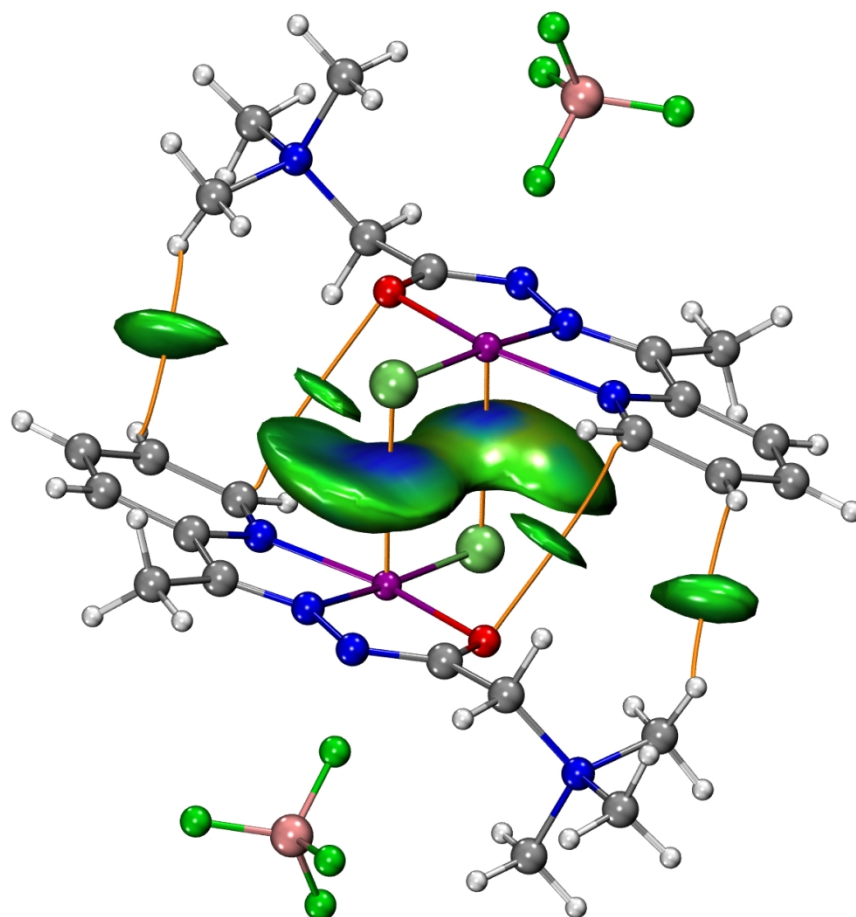


Figure 10a. IGM plots for 1--1

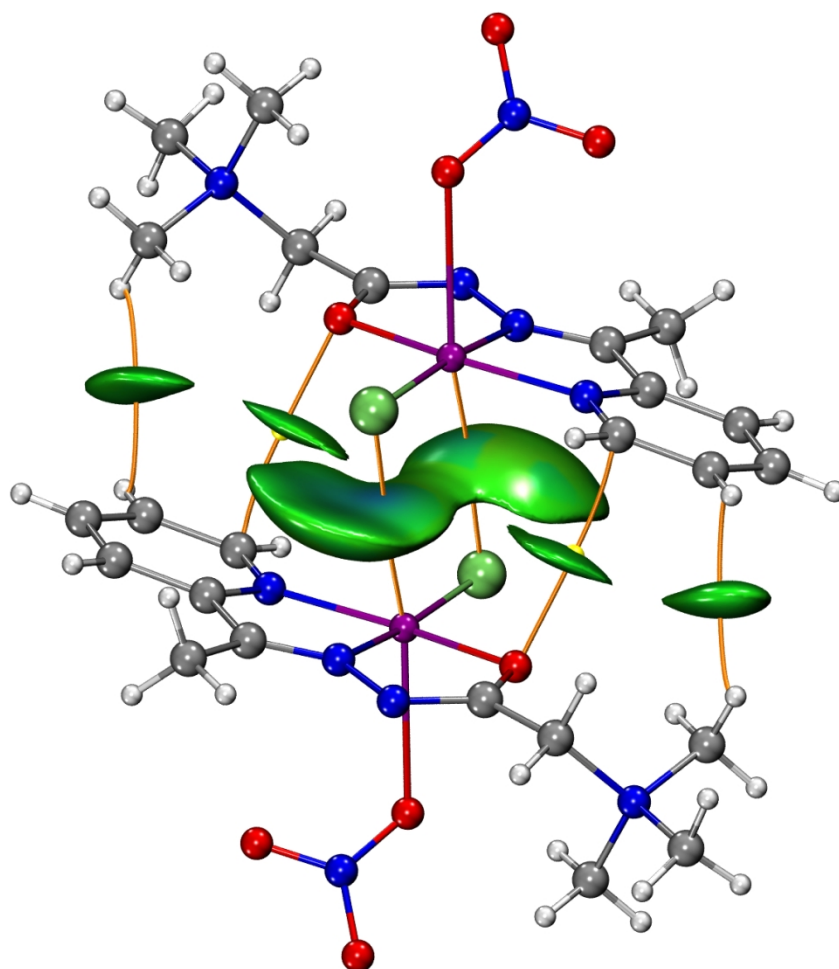


Figure 10b. IGM plots for 2--2

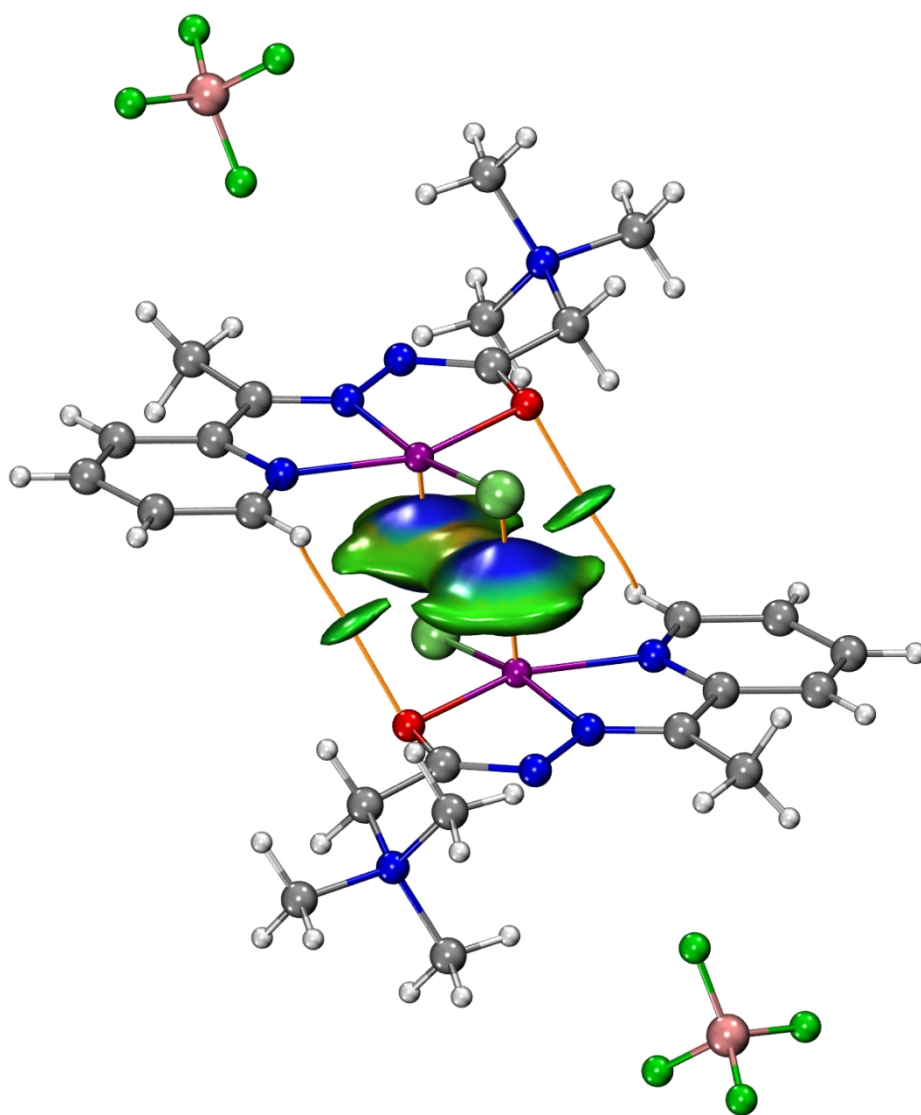


Figure 10c. IGM plots for 3--3

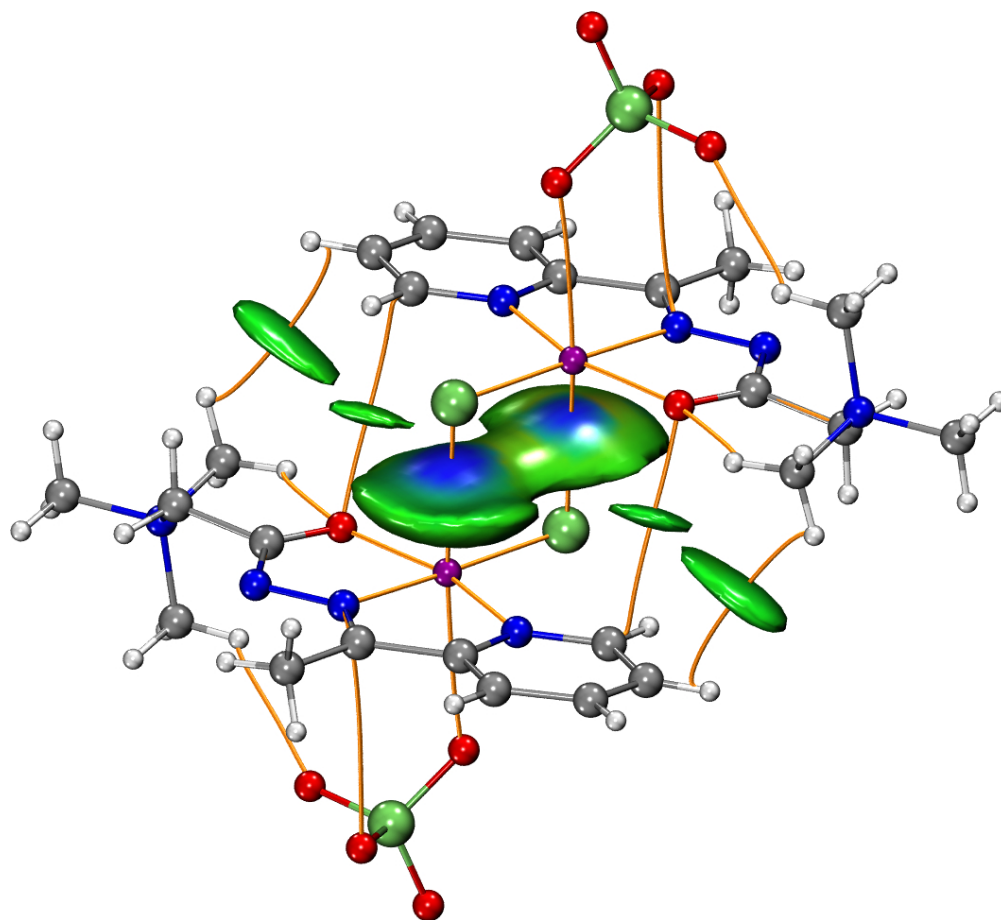


Figure 10d. IGM plots for 4--4